This article has been accepted for publication in a future issue of this journal, but has not been fully edited. Content may change prior to final publication. Citation information: DOI 10.1109/JSAC.2022.3143267, IEEE Journal on Selected Areas in Communications



# Adaptive Aggregate Transmission for Device-to-Multi-Device Aided Cooperative NOMA Networks

Yao Xu, Jie Tang, *Senior Member, IEEE*, Bo Li, *Member, IEEE*, Nan Zhao, *Senior Member, IEEE*, Dusit Niyato, *Fellow, IEEE*, Kai-Kit Wong, *Fellow, IEEE*

***Abstract*—The integration of device-to-device (D2D) communications with cooperative non-orthogonal multiple access (NOMA) can achieve superior spectral efficiency. However, the mutual interference caused by D2D communications may prevent NOMA from divering its high spectral efficiency advantage. Meanwhile, the low adaptability of the fixed transmission strategy can decrease the reliability of the cell-edge user (CEU). To further improve the spectral efficiency, we investigate a device-to-multi-device (D2MD) assisted cooperative NOMA system, where two cell-center users (CCUs) and one CEU are paired as a D2MD cluster. Specifically, the base station directly serves the two CCUs while communicating with the CEU via one CCU. Moreover, we propose an adaptive aggregate transmission scheme using dynamic superposition coding, pre-designing the decoding orders and prior information cancellation for the D2MD assisted cooperative NOMA system to enhance the reliability of the CEU. We provide the closed-form expressions for the outage probability, diversity order, outage throughput, ergodic sum capacity, average spectral efficiency, and spectral efficiency scaling over Nakagami-$m$ fading channels under perfect and imperfect successive interference cancellation. The numerical results validate the correctness of the analytical derivations and the effectiveness of the proposed scheme.**

***Index Terms*—Cooperative relaying, non-orthogonal multiple access, outage probability, spectral efficiency, imperfect successive interference cancellation.**

## I. Introduction

As a significant carrier of future communication services, the Internet of things (IoT) supported by intelligent terminal devices possesses extensive and diversified applications, such as industrial automation, massive machine-type communications and smart city [1], [2]. The high service quality required by the applications above imposes many severe challenges to the performance of future wireless networks, including ultra-high device access density and ultra-high spectral efficiency (SE) [3], [4]. Recently, non-orthogonal multiple access (NOMA) adopting successive interference cancellation (SIC) and superposition coding has raised considerable attention because it can achieve remarkable SE [5], [6]. Unlike orthogonal multiple access (OMA), NOMA actively introduces inter-user interference through resource sharing, and it performs SIC at the receiver to realize successful decoding for enhancing the overall system SE and providing massive connectivity [7], [8].

Due to the attractive SE superiority of NOMA, some researchers have integrated device-to-device (D2D) communications with NOMA to obtain superior performance gain [9]–[15]. Specifically, resource allocation optimization is a promising research direction for D2D-aided NOMA systems. In [9], Zhao *et al.* jointly optimized the subchannel and power allocation for a NOMA enhanced D2D system, where the D2D transmitter can use NOMA to communicate with multiple D2D receivers. In [10], Pei *et al.* proposed an iterative algorithm with low complexity to maximize the energy efficiency for D2D underlaying energy harvesting-based NOMA networks via the joint optimization of power control and time allocation. Pan *et al.* in [11] maximized the sum rate of D2D users for D2D underlaying NOMA-based systems by solving the channel assignment and power control problem. Zheng *et al.* in [12] investigated the power allocation and user clustering for D2D underlaid uplink NOMA networks. In [13], Dai *et al.* discussed the interlay and underlay modes for D2D-assisted NOMA networks and jointly designed the resource management and mode selection. In [14], a two-stage game approach was proposed by Li *et al.* to maximize the unilateral energy efficiency for D2D-assisted uplink NOMA systems. Moreover, Sun *et al.* in [15] proposed a traffic offloading scheme for D2D-enabled NOMA networks and maximized the capacity achieved by the D2D network using the optimization of power control and subchannel assignment.

### A. Related Work

To simultaneously acquire higher SE and broader coverage, cooperative relaying has also been applied to NOMA-based networks [16]–[28]. In [16], Ding *et al.* proposed a cooperative NOMA scheme using user prior information and designed a

Manuscript received August 12, 2021; revised October 29, 2021; accepted December 16, 2021. This work was supported by the National Natural Science Foundation of China under Grants 62171154, 61871065 and 61901137. (*Corresponding author: Bo Li.*)

Yao Xu and Bo Li are with the Communication Research Center, Harbin Institute of Technology, Harbin 150001, China (email: xuyao_hit@sina.com; libo1983@hit.edu.cn).

Jie Tang is with the School of Electronic and Information Engineering, South China University of Technology, Guangzhou 510641, China (e-mail: eejtang@scut.edu.cn).

Nan Zhao is with the School of Information and Communication Engineering, Dalian University of Technology, Dalian 116024, China (e-mail: zhaonan@dlut.edu.cn).

Dusit Niyato is with the School of Computer Science and Engineering, Nanyang Technological University, 639798, Singapore. (e-mail: dniyato@ntu.edu.sg).

Kai-Kit Wong is with the Department of Electronic and Electrical Engineering, University College London, London WC1E 6BT, U.K. (e-mail:kai-kit.wong@ucl.ac.uk).

user pairing strategy to reduce the system complexity. Based on this work, the influence of relay selection on cooperative NOMA was further investigated in [17]. Liu *et al.* applied simultaneous wireless information and power transfer (SWIPT) to cooperative NOMA in [18], where near users perform as energy harvesting relays to assist far users. A dynamic cooperative NOMA scheme was characterized for the multicast cognitive radio network by Lv *et al.* in [19] to attain better outage performance. Cao *et al.* analyzed the secrecy performance of the cooperative NOMA system with a multi-antenna full-duplex relay in [20]. In [21], Zhong *et al.* proposed a full-duplex relay-assisted cooperative NOMA scheme and validated the performance gain achieved by the proposed scheme over the half-duplex relay aided cooperative NOMA scheme. Si *et al.* studied a cooperative NOMA scheme using spatial modulation and SWIPT in [22], where the stronger user with energy harvesting and full-duplex characteristics helps the weaker user. In [23], joint beamforming and power-splitting control was proposed by Xu *et al.* to maximize the achievable data rate of the strong user for multiple-input single-output (MISO) and SWIPT-based cooperative NOMA systems. Qian *et al.* minimized the overall-latency of the cellular aided mobile edge computing system in [24], where spectrum sharing and NOMA are exploited to realize the cooperation between the cellular user and the edge-computing user. In [25], a joint power and time optimization was presented by Bae *et al.* to minimize the system outage probability of cooperative NOMA with a two-way relay. Moreover, Yuan *et al.* proposed an iterative algorithm using a successive convex approximation in [26] to optimize the system energy efficiency for full-duplex-based cooperative SWIPT NOMA systems. In [27], Zhou *et al.* investigated the beamforming design problems for cooperative MISO-NOMA cognitive radio networks using SWIPT to improve the security of the primary network. In [28], Wu *et al.* proposed the vertical decomposition and a layered-algorithm to maximize the overall throughput for the NOMA-based cooperative relaying system.

Although NOMA can improve the SE of the cooperative relaying system, the cooperative procedure inevitably suppresses the SE superiority of NOMA. Therefore, many research efforts have been devoted to combining D2D communications and cooperative NOMA to increase the SE and device access density [29]–[34]. In [29], Zhang *et al.* analyzed the outage probability for the proposed D2D-assisted cooperative NOMA scheme, where the near user acts as a full-duplex relay to help the far user. Kim *et al.* in [30] considered a D2D-aided cooperative NOMA system using the dedicated relay and presented a power allocation scheme to maximize the capacity scaling. In [31], Xu *et al.* evaluated the outage performance and outage throughput for the D2D aided uplink cooperative NOMA system. In [32], Li *et al.* proposed a D2D content sharing strategy for the cooperative NOMA system considering social ties and studied the performance in terms of the social-aware rates. Moreover, Kader *et al.* in [33] proposed a D2D-aided uplink cooperative NOMA system, where the near users can directly communicate with the base station (BS), and the far user connects with the BS with the aid of one near user. In [34], Zou *et al.* applied the D2D technology to a downlink coordinated direct and relay transmission (CDRT) system and validated the advantage of ergodic sum capacity over the OMA scheme.

### B. Motivation and Contributions

The use of D2D communications in cooperative NOMA can further improve the system SE. However, the introduction of D2D may cause mutual interference between D2D users and cellular users, and thus indirectly burying the high SE potential of NOMA. Meanwhile, in the D2D-assisted cooperative NOMA system, the low adaptability caused by the fixed transmission strategy can decrease the reliability of the cell-edge user (CEU) and system throughput. Currently, the existing works integrate D2D communications with cooperative NOMA and design a fixed transmission strategy to enhance the SE, but they ignore the measurement of the reliability of the CEU. Moreover, the existing studies only consider a simple channel model (i.e., Rayleigh fading channels) and perfect SIC, which is not realistic in practical applications. Motivated by these observations, considering Nakagami-$m$ fading channels and imperfect SIC, we investigate a device-to-multi-device (D2MD) assisted cooperative NOMA system. Besides, we propose an adaptive aggregate transmission scheme using dynamic superposition coding, pre-designing the decoding orders and prior information cancellation. It is worth noting that D2MD is a one-to-many D2D communication type, and one D2D transmitter can simultaneously broadcast data to several D2D receivers in a D2MD cluster [35]. The proposed system model can be treated as Scenario 2B in [35], which is a critical 3GPP D2D communication scenario. Moreover, the proposed scheme can be applied to other practical application scenarios such as the general cellular network and light IoT network.

The contributions of this paper are summarized as follows.

- The existing D2D-assisted cooperative NOMA schemes using a fixed transmission strategy may reduce the reliability of the CEU and cannot provide sufficient design space to improve SE. To cope with this issue, we first present a D2MD assisted downlink cooperative NOMA system consisting of one BS, one CEU and two cell-center users (CCUs), where these three users are paired as a D2MD cluster. Specifically, the BS can directly communicate with the CCUs while connecting with the CEU via one CCU.
- To further enhance the SE and the reliability of the CEU, we propose an adaptive aggregate transmission scheme by adopting the prior information cancellation and designing dynamic superposition coding and decoding orders. The proposed scheme can be straightforwardly extended to the massive-user or multi-cell scenarios by using user pairing and hybrid multiple access.
- We characterize the performance of the proposed scheme in terms of communication reliability and effectiveness. Specifically, the closed-form expressions for the outage probability, outage throughput, ergodic sum capacity, and average SE are derived over Nakagami-$m$ fading channels with imperfect SIC.

- To gain more insights, we analyze the asymptotic performance for the outage probability and average SE in the high transmit power region. Based on this, the diversity order and SE scaling achieved by the proposed scheme are further investigated.
- Compared with the conventional D2D-assisted CDRT (D-CDRT) scheme, the proposed scheme can transmit more data streams with the same amount of time resource. The proposed scheme can achieve better outage performance of the CEU, outage throughput and average SE under perfect and imperfect SIC. The SE superiority of the proposed scheme over OMA comparisons with perfect SIC is validated through simulations. Moreover, we study the impact of some practical factors, including fading parameters, distance settings and imperfect SIC on the average SE.

### C. Organization

The rest of the paper is organized as follows. Section II introduces the system model of D2MD-assisted cooperative NOMA. Section III presents the design of the proposed adaptive aggregate scheme. In Section IV, the closed-form expressions for the outage probability, outage throughput, diversity order, ergodic sum capacity, average SE, and SE scaling are derived. Numerical results and conclusions are provided in Section V and Section VI, respectively.

*Notations*: In this paper, $F_Z(z)$ and $f_Z(z)$ represent the cumulative distribution function (CDF) and the probability density function (PDF) of the variable $Z$, respectively; the meaning of the operator $\mathbb{E}(\cdot)$ is to obtain the expectation value; the operation $\Xi' \Rightarrow \Xi(z \to z')$ denotes that $\Xi'$ can be obtained by replacing $z$ with $z'$; "$\to$" means "approaching" and "$\sim$" represents "be proportional to".

## II. System Model

We consider a downlink D2MD-enabled cooperative NOMA system shown in Fig. 1, where the BS can directly communicate with two CCUs (i.e., $U_1$ and $U_2$) while serving a CEU (i.e., $U_3$) via a decode-and-forward relaying user (i.e., $U_2$) due to the significant obstacle between the BS and $U_3$ [1]. Specifically, the system model consists of a D2MD cluster, in which $U_2$ is a potential D2D transmitter, and $U_1$ and $U_3$ are within the proximity detection region of $U_2$. All nodes have a single antenna and operate in half-duplex mode. Hereafter, let subscripts $s$, 1, 2, and 3 denote the BS, $U_1$, $U_2$ and $U_3$, respectively. Assume that each channel link is subject to independent Nakagami-$m$ block fading, and all the receiver nodes suffer from the additive white Gaussian noise with zero mean and variance $N_0$. The block fading means the channel changes over different blocks while remaining constant within one block. To reduce the system complexity, we can easily extend the proposed system model to the massive-user or multi-cell scenarios via the existing user pairing and hybrid multiple access in [36].

[1]Although a three-user system is investigated in this paper, the proposed scheme can be directly applied to a multi-user system (i.e., more than three users) by using user pairing. For instance, the existing user pairing methods in [18] and [36] can group users. Then the conventional orthogonal multiple access is used to distinguish different user pairs, and the proposed scheme is performed in each group [36]. Using user pairing can effectively reduce the system complexity and inter-user interference for NOMA-based systems [37]. Besides, the analysis can also be directly extended to a multi-user system by using the random near user and random far user selection method in [18].

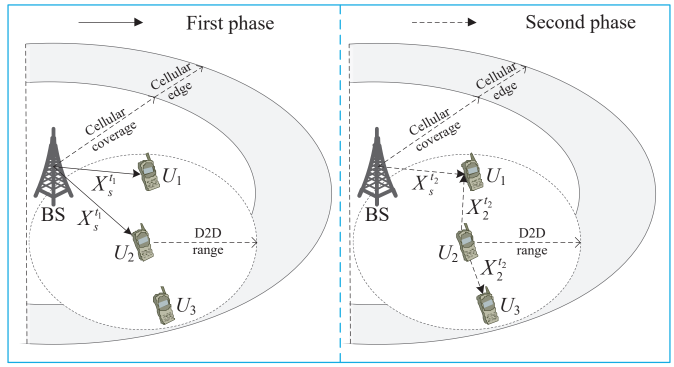


Fig. 1. System model. An illustration of the proposed adaptive aggregate transmission scheme for the D2MD assisted cooperative NOMA system with one BS, two CCUs and one CEU.

The channel coefficient, channel gain and fading parameter between $x$ and $y$ are denoted by $h_{xy}$, $\lambda_{xy}$ and $m_{xy}$, respectively, where $x, y \in \{s, 1, 2, 3\}$, $x \neq y$. The expectation of $\lambda_{xy}$ is $\Omega_{xy} = G_0 {d_{xy}}^{-\alpha_0}$, where $\alpha_0$ and $G_0$ represent the path loss exponent and the channel gain for reference distance (i.e., 1 m), respectively, and $d_{xy}$ denotes the distance between $x$ and $y$. In this paper, we assume that $d_{s1} < d_{s2}$ and $d_{23} < d_{21}$, which may not satisfy $\lambda_{s1} > \lambda_{s2}$ and $\lambda_{23} > \lambda_{21}$. Note that the proposed scheme can be directly used in practical application if a feasibility-check procedure is performed to ensure the above distance conditions. Moreover, the proposed scheme can also be easily extended to other distance assumptions via downlink NOMA.

## III. Adaptive Aggregate Transmission Scheme

To offload the data traffic and improve the SE, we propose an adaptive transmission scheme for the D2MD-enabled cooperative NOMA system. One transmission block is divided into two consecutive and equal phases in the proposed scheme to complete downlink NOMA and D2D multicast transmissions, as detailed below.

### A. First Phase

In the first phase (i.e., $t_1$), the BS broadcasts the signal $X_s^{t_1} = \sum_{i=1}^{3} \sqrt{a_i P_s} x_i$ to $U_1$ and $U_2$ using power-domain superposition coding, where $P_s$ is the transmit power of the BS, the signal $x_i$ contains the required information for $U_i$, $i \in \{1, 2, 3\}$, and $a_i$ represents the corresponding power allocation coefficient. Since the condition $d_{s1} < d_{s2}$ holds and $U_3$ is a CEU, the power allocation coefficient should satisfy $\sum_{i=1}^{3} a_i = 1$ and $a_3 > a_2 > a_1$. The received signals at $U_j$, $j \in \{1, 2\}$, can be written as

$$Y_j^{t_1} = h_{sj} X_s^{t_1} + n_j^{t_1}, \tag{1}$$

where $n_i^{t_k} \sim \mathcal{CN}(0, N_0)$, $k \in \{1, 2\}$, denotes the complex additive white Gaussian noise at the receiver $U_i$ in $t_k$.

The CCU $U_2$ first decodes $x_3$ by treating $x_1$ and $x_2$ as noise, and then cancels $x_3$ and performs SIC to decode $x_2$ by treating $x_1$ as noise. Note that, based on downlink NOMA, $U_2$ does not need to decode $x_1$ in the first phase. Meanwhile, the CCU $U_1$ uses SIC to decode $x_3$, $x_2$ and $x_1$ sequentially. Therefore, the received signal-to-interference-and-noise ratios at $U_j$, $j \in \{1,2\}$, for decoding $x_3$ and $x_2$ in $t_1$ can be respectively expressed as

$$\gamma_{j,x_3}^{t_1} = \frac{\lambda_{sj} a_3 \rho_s}{\lambda_{sj}\left(a_1 + a_2\right)\rho_s + 1}, \tag{2}$$

$$\gamma_{j,x_2}^{t_1} = \frac{\lambda_{sj} a_2 \rho_s}{\lambda_{sj}\left(a_1 + \kappa_{j,1}^{t_1} a_3\right)\rho_s + 1}, \tag{3}$$

where the transmit signal-to-noise ratio (SNR) $\rho_s$ is denoted as $\rho_s = \frac{P_s}{N_0}$, and the fractional error factor $\kappa_{j,1}^{t_1}$ represents the residual interference levels for imperfect SIC. Specifically, the value range of the fractional error factor is from zero to one. The factor value equals zero means that perfect SIC is performed, while the factor value equals one represents that no SIC is performed. Moreover, the received signal-to-interference-and-noise ratio at $U_1$ for decoding $x_1$ in $t_1$ can be expressed as

$$\gamma_{1,x_1}^{t_1} = \frac{\lambda_{s1} a_1 \rho_s}{\lambda_{s1}\left(\kappa_{1,2}^{t_1} a_2 + \kappa_{1,3}^{t_1} a_3\right)\rho_s + 1}, \tag{4}$$

where $\kappa_{1,2}^{t_1}$ and $\kappa_{1,3}^{t_1}$ are the fractional error factors.

### *B. Second Phase*

Since $U_1$ and $U_2$ cannot always decode $x_3$ successfully in the first phase, we propose an adaptive transmission scheme to improve the SE. Moreover, the predetermined decoding order is designed to reduce the decoding complexity while guaranteeing the reliability of the CEU.

Let the binary numbers $A_1$ and $A_2$ represent the decoding results for $x_3$ at $U_1$ and $U_2$ in $t_1$, respectively, where $A_j = 0$ and $A_j = 1$, $j \in \{1,2\}$, denote failed decoding and successful decoding, respectively. A two-bit binary number $A = A_1 A_2$ indicates the combination of two outage events. For instance, "$A = 3$ (decimal form)" denotes the event that both $U_1$ and $U_2$ can decode $x_3$ successfully in the first phase.

During the second phase (i.e., $t_2$), the BS transmits $X_s^{t_2} = \sqrt{P_s} x_1'$ to $U_1$, where $x_1'$ is a new downlink signal required by $U_1$. Meanwhile, $U_2$ attempts to forward $x_3$ to $U_3$ as a decode-and-forward relay while acting as a D2D transmitter to communicate with $U_1$ and $U_3$ via NOMA-based D2D multicast communication. Specifically, the user $U_2$ broadcasts a superposed signal $X_2^{t_2}$ for case $A$, and $X_2^{t_2}$ can be expressed as

$$X_2^{t_2} = \sqrt{b_1^A P_u} x_{d_1} + \sqrt{b_2^A P_u} x_{d_3} + \sqrt{b_3^A P_u} x_3, \tag{5}$$

where $x_{d_1}$ and $x_{d_3}$ are the desired D2D signal for $U_1$ and $U_3$, respectively, $P_u$ is the transmit power of $U_2$, and $b_i^A, i \in \{1,2,3\}$ is the power allocation coefficient with $\sum_{i=1}^{3} b_i^A = 1$. Due to $d_{23} < d_{21}$ and the cooperative transmission of $x_3$, the power allocation coefficients should satisfy $1 > b_1^A > b_3^A > b_2^A > 0$ via downlink NOMA when $U_2$ can decode $x_3$ successfully in the first phase (i.e. $A = 1,3$). Conversely, if $U_2$ cannot decode $x_3$ in the first phase (i.e., $A = 0,2$), the power allocation coefficient $b_3^A$ in (5) should be set to $b_3^A = 0$. Meanwhile, based on downlink NOMA, the power allocation coefficients $b_1^A$ and $b_2^A$ should satisfy $1 > b_1^A > b_2^A > 0$. Therefore, the received signals at $U_1$ and $U_3$ in the second phase can be respectively expressed as

$$\begin{aligned} Y_{1,A}^{t_2} =& h_{21}\left(\sqrt{b_1^A P_u} x_{d_1} + \sqrt{b_2^A P_u} x_{d_3} + \sqrt{\varpi^A b_3^A P_u} x_3\right) \\ &+ h_{s1}\sqrt{P_s} x_1' + n_1^{t_2}, \end{aligned} \tag{6}$$

$$\begin{aligned} Y_{3,A}^{t_2} =& h_{23}\left(\sqrt{b_1^A P_u} x_{d_1} + \sqrt{b_2^A P_u} x_{d_3} + \sqrt{b_3^A P_u} x_3\right) \\ &+ n_3^{t_2}, \end{aligned} \tag{7}$$

where the flag value $\varpi^A \in \{0,1\}$ indicates whether the interference term $\sqrt{b_3^A P_u} x_3$ in (6) exists.

When both $U_1$ and $U_2$ can decode $x_3$ successfully in the first phase (i.e., $A = 3$), $U_1$ can estimate $\sqrt{b_3^A P_u}$ in the second phase and use the decoded $x_3$ to cancel the interference $\sqrt{b_3^A P_u} x_3$ in (6). Therefore, the flag value $\varpi^A$ should satisfy $\varpi^0 = \varpi^2 = \varpi^3 = 0$ and $\varpi^1 = 1$.

The received signals in (6) and (7) contain multiple signal components, which means that the diversity and uncertainty of decoding orders at $U_1$ and $U_3$ in the second phase may cause high complexity in practical implementation. To cope with this issue, we propose a predetermined decoding order strategy via power allocation coefficient design. Specifically, the D2D transmission is typically over the short distance, and thus the condition $\Omega_{s1} < \Omega_{21}$ is more general than $\Omega_{s1} > \Omega_{21}$ in practice. In the proposed strategy, $U_2$ first attains statistical channel information $\Omega_{s1}$ and $\Omega_{s1}$ by using a two-step channel estimation [37]. Then, the power allocation coefficient is designed as $b_1^A > \frac{\Omega_{s1}}{\Omega_{21}\alpha} > \max\{b_2^A, b_3^A\}$ at $U_2$, where $\alpha \triangleq \frac{P_u}{P_s}$ is a scale factor. Therefore, $U_1$ can use SIC to decode $x_{d_1}$ and $x_1'$ sequentially by treating the non-decoded signals as noise, while the decoding order at $U_3$ in the second phase is pre-determined as $x_{d_1}$, $x_3$ and $x_{d_3}$. The received signal-to-interference-and-noise ratios for $U_1$ to decode $x_{d_1}$ and $x_1'$ in case $A$ can be respectively expressed as

$$\gamma_{1,x_{d_1}}^{t_2,A} = \frac{\lambda_{21} b_1^A \alpha \rho_s}{\lambda_{s1}\rho_s + \lambda_{21}\left(b_2^A + \varpi^A b_3^A\right)\alpha\rho_s + 1}, \tag{8}$$

$$\gamma_{1,x_1'}^{t_2,A} = \frac{\lambda_{s1}\rho_s}{\lambda_{21}\left(\kappa_{1,1}^{t_2,A} b_1^A + b_2^A + \varpi^A b_3^A\right)\alpha\rho_s + 1}, \tag{9}$$

where $\kappa_{1,1}^{t_2,A}$ is a fractional error factor.

Moreover, the received signal-to-interference-and-noise ratios for $U_3$ to decode $x_{d_1}$, $x_3$ and $x_{d_3}$ in case $A$ can be expressed as

$$\gamma_{3,x_{d_1}}^{t_2,A} = \frac{\lambda_{23} b_1^A \alpha \rho_s}{\lambda_{23}\left(b_2^A + b_3^A\right)\alpha\rho_s + 1}, \tag{10}$$

$$\gamma_{3,x_3}^{t_2,A} = \frac{\lambda_{23} b_3^A \alpha \rho_s}{\lambda_{23}\left(\kappa_{3,1}^{t_2,A} b_1^A + b_2^A\right)\alpha\rho_s + 1}, \tag{11}$$

$$\gamma_{3,x_{d_3}}^{t_2,A} = \frac{\lambda_{23} b_2^A \alpha \rho_s}{\lambda_{23}\left(\kappa_{3,2}^{t_2,A} b_1^A + \kappa_{3,3}^{t_2,A} b_3^A\right)\alpha\rho_s + 1}, \tag{12}$$

where $\kappa_{3,1}^{t_2,A}$, $\kappa_{3,2}^{t_2,A}$ and $\kappa_{3,3}^{t_2,A}$ represent fractional error factors.

Based on (4), (9) and (12), the achievable rate for the data streams of $x_1$, $x_1'$ and $x_{d_3}$ can be respectively expressed as

$$C_{x_1} = \frac{1}{2}\log_2\left(1+\gamma_{1,x_1}^{t_1}\right), \tag{13}$$

$$C_{x_1'}^{A} = \frac{1}{2}\log_2\left(1+\gamma_{1,x_1'}^{t_2,A}\right), \tag{14}$$

$$C_{x_{d_3}}^{A} = \frac{1}{2}\log_2\left(1+\gamma_{3,x_{d_3}}^{t_2,A}\right). \tag{15}$$

To perform SIC, $U_1$ needs to decode $x_2$ in the first phase and $U_3$ must decode $x_{d_1}$ during the second phase. Therefore, based on (3), (8) and (10), the achievable rate for the data streams of $x_2$ and $x_{d_1}$ can be respectively expressed as

$$C_{x_2} = \frac{1}{2}\log_2\left(1+\min\left\{\gamma_{1,x_2}^{t_1},\gamma_{2,x_2}^{t_1}\right\}\right), \tag{16}$$

$$C_{x_{d_1}}^{A} = \frac{1}{2}\log_2\left(1+\min\left\{\gamma_{1,x_{d_1}}^{t_2,A},\gamma_{3,x_{d_1}}^{t_2,A}\right\}\right). \tag{17}$$

The first-link and second-link achievable rates of $x_3$ at $U_2$ and $U_3$ are $\frac{1}{2}\log_2\left(1+\gamma_{2,x_3}^{t_1}\right)$ and $\frac{1}{2}\log_2\left(1+\gamma_{3,x_3}^{t_2,A}\right)$, respectively. Meanwhile, the achievable rate of $x_3$ at $U_1$ in the first phase is $\frac{1}{2}\log_2\left(1+\gamma_{1,x_3}^{t_1}\right)$. The achievable rate of cooperative decode-and-forward relaying is dominated by the worst link, and $U_1$ must decode $x_3$ for SIC in the first phase [38]. Therefore, using [38, eq. (5)], (2) and (11), we can express the achievable rate for $x_3$ as

$$C_{x_3}^{A} = \frac{1}{2}\log_2\left(1+\min\left\{\gamma_{1,x_3}^{t_1},\gamma_{2,x_3}^{t_1},\gamma_{3,x_3}^{t_2,A}\right\}\right). \tag{18}$$

## IV. Performance Analysis

This section investigates the performance for the proposed scheme over Nakagami-$m$ fading channels. Due to the adaptive characteristics of the proposed scheme, the performance analysis is quite difficult. In view of this, we use classification discussion and approximation method to obtain closed-form of various metrics for proving the effectiveness of the proposed scheme and the scarcity of analysis. Specifically, the closed-form expressions for the outage probability and outage throughput of the proposed scheme are derived when the target data rates are fixed beforehand to satisfy the quality of service. Conversely, we use the ergodic sum capacity and average SE to evaluate the performance of the proposed scheme if the target rates change dynamically according to the channel qualities. Similar to [8], the following derivations can provide guidance for system optimization, such as SE maximization.

### A. Outage Probability and Outage Throughput

The event that the receiver node $y$ can decode the signal $\bar{y}$ successfully in the first phase is denoted by $E_{y,\bar{y}}^{t_1} \triangleq \left\{\frac{1}{2}\log(1+\gamma_{y,\bar{y}}^{t_1}) > R_{\bar{y}}\right\}$. Similarly, the inequality $E_{z,\bar{z}}^{t_2,A} \triangleq \left\{\frac{1}{2}\log(1+\gamma_{z,\bar{z}}^{t_2,A}) > R_{\bar{z}}\right\}$ represents that the signal $\bar{z}$ can be decoded at the receiver node $z$ in $t_2$ for case $A$, where $y \in \{1,2\}$, $\bar{y} \in \{x_1,x_2,x_3\}$, $z \in \{2,3\}$, $\bar{z} \in \{x_3,x_1',x_{d_1},x_{d_3}\}$, and $R_{\bar{y}}$ and $R_{\bar{z}}$ are the target data rates of $\bar{y}$ and $\bar{z}$, respectively. The complement sets of $E_{y,\bar{y}}^{t_1}$ and $E_{z,\bar{z}}^{t_2,A}$ are denoted as $\tilde{E}_{y,\bar{y}}^{t_1}$ and $\tilde{E}_{z,\bar{z}}^{t_2,A}$, respectively. Moreover, let $\varphi_{\bar{y}} \triangleq 2^{R_{\bar{y}}}-1$ and $\varphi_{\bar{z}} \triangleq 2^{R_{\bar{z}}}-1$.

Before decoding $x_1$, $U_1$ must sequentially decode $x_3$ and $x_2$ first. Therefore, we can use (2), (3) and (4) to calculate the outage probability for $U_1$ to decode $x_1$ in the first phase as

$$\begin{aligned} P_{1,\text{out}}^{t_1,x_1} &= 1-\Pr\left(E_{1,x_3}^{t_1}\cap E_{1,x_2}^{t_1}\cap E_{1,x_1}^{t_1}\right) \\ &= 1-\Pr\left(\lambda_{s1} > \max\{\phi_1,\phi_2,\phi_3\}\right) \\ &= F_{\lambda_{s1}}\left(\tilde{\phi}_1\right), \end{aligned} \tag{19}$$

where $\tilde{\phi}_1 = \max\{\phi_1,\phi_{2,1},\phi_3\}$, $\phi_{2,j} = \frac{\varphi_{x_2}}{\rho_s\left(a_2-\left(a_1+\kappa_{j,1}^{t_1}a_3\right)\varphi_{x_2}\right)}$ and $\phi_3 = \frac{\varphi_{x_3}}{\rho_s\left(a_3-(a_1+a_2)\varphi_{x_3}\right)}$. Note that the conditions $\phi_1 > 0$, $\phi_{2,j} > 0$ and $\phi_3 > 0$ should be guaranteed via power allocation coefficient design to implement NOMA successfully in practice. Moreover, $F_{\lambda_{s1}}(\cdot)$ denotes the CDF of the variable $\lambda_{s1}$ with Gamma distribution. Specifically, if the channel coefficient $h_{xy}$ follows Nakagami-$m$ distribution, the CDF of the channel gain $\lambda_{xy}$ exhibiting Gamma distribution can be written as

$$F_{\lambda_{xy}}(z) = 1-\exp\left(-\frac{zm_{xy}}{\Omega_{xy}}\right)\sum_{i=0}^{m_{xy}-1}\frac{1}{i!}\left(\frac{zm_{xy}}{\Omega_{xy}}\right)^i. \tag{20}$$

Since $U_2$ must adopt SIC to decode $x_2$ after decoding $x_3$, we can use (2) and (3) to calculate the outage probability for $U_2$ to decode $x_2$ during the first phase as

$$\begin{aligned} P_{2,\text{out}}^{t_1,x_2} &= 1-\Pr\left(E_{2,x_3}^{t_1}\cap E_{2,x_2}^{t_1}\right) \\ &= 1-\Pr\left(\lambda_{s2} > \max\left\{\phi_{2,2},\phi_3\right\}\right) \\ &= F_{\lambda_{s2}}\left(\tilde{\phi}_2\right), \end{aligned} \tag{21}$$

where $\tilde{\phi}_2 = \max\{\phi_{2,2},\phi_3\}$.

Based on the proposed scheme, $U_3$ may decode $x_3$ successfully in two cases (i.e., $A=1,3$). Therefore, the outage probability for $U_3$ to decode $x_3$ in the second phase can be expressed as

$$P_{3,\text{out}}^{t_2,x_3} = 1-\sum\nolimits_{\bar{k}=1,3}\mathbb{P}_{3,\bar{k}}^{t_2,x_3}, \tag{22}$$

where $\mathbb{P}_{3,\bar{k}}^{t_2,x_3} = \Pr(A=\bar{k})\Pr(E_{3,x_{d_1}}^{t_2,\bar{k}}\cap E_{3,x_3}^{t_2,\bar{k}}|A=\bar{k})$.

Using $\gamma_{1,x_3}^{t_1}$, $\gamma_{2,x_3}^{t_1}$, $\gamma_{3,x_{d_1}}^{t_2,1}$ and $\gamma_{3,x_3}^{t_2,1}$, we can calculate $\mathrm{P}_{3,1}^{t_2,x_3}$ as

$$\begin{aligned} \mathbb{P}_{3,1}^{t_2,x_3} &= \Pr\left(\lambda_{s1} < \phi_3, \lambda_{s2} > \phi_3, \lambda_{23} > \tilde{\phi}_3^1\right) \\ &= F_{\lambda_{s1}}(\phi_3)\left(1-F_{\lambda_{s2}}(\phi_3)\right)\left(1-F_{\lambda_{23}}\left(\tilde{\phi}_3^1\right)\right), \end{aligned} \tag{23}$$

where $\tilde{\phi}_3^A = \max\left\{\phi_4^A,\phi_6^A\right\}$, $\phi_4^A = \frac{\varphi_{x_{d_1}}}{\alpha\rho_s\left(b_1^A-\left(b_2^A+b_3^A\right)\varphi_{x_{d_1}}\right)}$ and $\phi_6^A = \frac{\varphi_{x_3}}{\alpha\rho_s\left(b_3^A-\left(\kappa_{3,1}^{t_2,A}b_1^A+b_2^A\right)\varphi_{x_3}\right)}$. The inequalities $\phi_4^A > 0$ and $\phi_6^A > 0$ should be satisfied to apply NOMA successfully. Otherwise, the outage probability for $U_3$ to decode $x_3$ is always one.

Similarly, based on $\gamma_{1,x_3}^{t_1}$, $\gamma_{2,x_3}^{t_1}$, $\gamma_{3,x_{d_1}}^{t_2,3}$ and $\gamma_{3,x_3}^{t_2,3}$, the non-outage probability $\mathbb{P}_{3,3}^{t_2,x_3}$ can be calculated as

$$\begin{aligned} \mathbb{P}_{3,3}^{t_2,x_3} &= \Pr\left(\lambda_{s1} > \phi_3, \lambda_{s2} > \phi_3, \lambda_{23} > \tilde{\phi}_3^3\right) \\ &= \left(1-F_{\lambda_{s1}}(\phi_3)\right)\left(1-F_{\lambda_{s2}}(\phi_3)\right)\left(1-F_{\lambda_{23}}\left(\tilde{\phi}_3^3\right)\right). \end{aligned} \tag{24}$$

This article has been accepted for publication in a future issue of this journal, but has not been fully edited. Content may change prior to final publication. Citation information: DOI 10.1109/JSAC.2022.3143267, IEEE Journal on Selected Areas in Communications



Substituting (23) and (24) into (22), we obtain $P_{3,\text{out}}^{t_2,x_3}$ .

According to the proposed scheme, $U_1$ may decode $x_{d_1}$ successfully in four cases (i.e., $A=0,1,2,3$). Therefore, the outage probability for $U_1$ to decode $x_{d_1}$ during the second phase can be expressed as

$$P_{1,\text{out}}^{t_2,x_{d_1}}=1-\sum\nolimits_{\bar{k}=0}^{3}\mathbb{P}_{1,\bar{k}}^{t_2,x_{d_1}}, \tag{25}$$

where $\mathbb{P}_{1,\bar{k}}^{t_2,x_{d_1}}=\Pr(A=\bar{k})\Pr(E_{1,x_{d_1}}^{t_2,\bar{k}}|A=\bar{k})$.

For simplicity, applying [39, eq. (3.351.1)] to the following integral, we define

$$\begin{aligned}\mathcal{L}_1(\eta^*,\eta,\mu)&\triangleq\int_0^{\eta^*}z^{\eta}\exp(-\mu z)dz\\&=\frac{\eta!}{\mu^{\eta+1}}-\exp\left(-\eta^*\mu\right)\sum\nolimits_{\varepsilon_1=0}^{\eta}\frac{\eta!{\eta^*}^{\varepsilon_1}}{\varepsilon_1!\mu^{\eta-\varepsilon_1+1}}.\end{aligned} \tag{26}$$

Based on (20) and (26), we can use $\gamma_{1,x_3}^{t_1}$, $\gamma_{2,x_3}^{t_1}$, $\gamma_{1,x_{d_1}}^{t_2,0}$ and the binomial expansion of $(x+{\rho_s}^{-1})^i=\sum_{i_1=0}^{i}\binom{i}{i_1}{\rho_s}^{i_1-i}x^{i_1}$ to calculate $\mathbb{P}_{1,0}^{t_2,x_{d_1}}$ as

$$\begin{aligned}\mathbb{P}_{1,0}^{t_2,x_{d_1}}&=\Pr\left(\lambda_{s1}<\phi_3,\lambda_{s2}<\phi_3,\lambda_{21}>\lambda_{s1}\rho_s\phi_5^0+\phi_5^0\right)\\&=\mathcal{L}_1\left(\phi_3,i_1+m_{s1}-1,\frac{m_{s1}}{\Omega_{s1}}+\frac{m_{21}\rho_s\phi_5^0}{\Omega_{21}}\right)\\&\quad\times F_{\lambda_{s2}}\left(\phi_3\right)\Delta_i^0,\end{aligned} \tag{27}$$

where

$$\phi_5^A=\frac{\varphi_{x_{d_1}}}{\alpha\rho_s(b_1^A-(b_2^A+\varpi^Ab_3^A)\varphi_{x_{d_1}})}, \tag{28a}$$

$$\begin{aligned}\Delta_i^A=&\frac{{m_{s1}}^{m_{s1}}}{{\Omega_{s1}}^{m_{s1}}\Gamma(m_{s1})}\sum\nolimits_{i=0}^{m_{21}-1}\sum\nolimits_{i_1=0}^{i}\binom{i}{i_1}\frac{{\rho_s}^{i_1}}{i!}\\&\times\left(\frac{m_{21}\phi_5^A}{\Omega_{21}}\right)^i\exp\left(-\frac{m_{21}\phi_5^A}{\Omega_{21}}\right),\end{aligned} \tag{28b}$$

where $\Gamma(\cdot)$ is the Gamma function. Note that the condition $\phi_5^A>0$ should be met to implement NOMA successfully in practice.

Following the same steps in (27), we can obtain $\mathbb{P}_{1,1}^{t_2,x_{d_1}}$ as

$$\begin{aligned}\mathbb{P}_{1,1}^{t_2,x_{d_1}}&=\Pr(\lambda_{s1}<\phi_3,\lambda_{s2}>\phi_3,\lambda_{21}>\lambda_{s1}\rho_s\phi_5^1+\phi_5^1)\\&=\mathcal{L}_1\left(\phi_3,i_1+m_{s1}-1,\frac{m_{s1}}{\Omega_{s1}}+\frac{m_{21}\rho_s\phi_5^1}{\Omega_{21}}\right)\\&\quad\times\left(1-F_{\lambda_{s2}}\left(\phi_3\right)\right)\Delta_i^1.\end{aligned} \tag{29}$$

Moreover, using $\gamma_{1,x_3}^{t_1}$, $\gamma_{2,x_3}^{t_1}$, $\gamma_{1,x_{d_1}}^{t_2,2}$ and binomial expansion, we can calculate $\mathbb{P}_{1,2}^{t_2,x_{d_1}}$ as

$$\begin{aligned}\mathbb{P}_{1,2}^{t_2,x_{d_1}}&=\Pr\left(\lambda_{s1}>\phi_3,\lambda_{s2}<\phi_3,\lambda_{21}>\lambda_{s1}\rho_s\phi_5^2+\phi_5^2\right)\\&=\mathcal{L}_2\left(\phi_3,i_1+m_{s1}-1,\frac{m_{s1}}{\Omega_{s1}}+\frac{m_{21}\rho_s\phi_5^2}{\Omega_{21}}\right)\\&\quad\times F_{\lambda_{s2}}\left(\phi_3\right)\Delta_i^2,\end{aligned} \tag{30}$$

where the function $\mathcal{L}_2$ follows [39, eq. (3.351.2)] with

$$\begin{aligned}\mathcal{L}_2\left(C,\eta,\mu\right)&\triangleq\int_C^{\infty}z^{\eta}\exp\left(-\mu z\right)dz\\&=\exp\left(-C\mu\right)\sum\nolimits_{\varepsilon_1=0}^{\eta}\frac{\eta!C^{\varepsilon_1}}{\varepsilon_1!\mu^{\eta-\varepsilon_1+1}}.\end{aligned} \tag{31}$$

Similar to (30), we can use $\gamma_{1,x_3}^{t_1}$, $\gamma_{2,x_3}^{t_1}$, $\gamma_{1,x_{d_1}}^{t_2,3}$ and binomial expansion to obtain $\mathbb{P}_{1,3}^{t_2,x_{d_1}}$ as

$$\begin{aligned}\mathbb{P}_{1,3}^{t_2,x_{d_1}}&=\Pr\left(\lambda_{s1}>\phi_3,\lambda_{s2}>\phi_3,\lambda_{21}>\lambda_{s1}\rho_s\phi_5^3+\phi_5^3\right)\\&=\mathcal{L}_2\left(\phi_3,i_1+m_{s1}-1,\frac{m_{s1}}{\Omega_{s1}}+\frac{m_{21}\rho_s\phi_5^3}{\Omega_{21}}\right)\\&\quad\times(1-F_{\lambda_{s2}}(\phi_3))\Delta_i^3.\end{aligned} \tag{32}$$

Combining (25), (27), (29), (30) and (32), we obtain $P_{1,\text{out}}^{t_2,x_{d_1}}$.

*Theorem 1:* The outage probability for $U_1$ to decode $x_1'$ in the second phase can be written as

$$P_{1,\text{out}}^{t_2,x_1'}=1-\sum\nolimits_{\bar{k}=0}^{3}\mathbb{P}_{1,\bar{k}}^{t_2,x_1'}, \tag{33}$$

where

$$\begin{aligned}\mathbb{P}_{1,0}^{t_2,x_1'}=&\Bigg\{\Delta_{j_1}^0\Bigg(\mathcal{L}_1\left(\phi_3,j_1+m_{s1}-1,\frac{m_{21}\phi_5^0\rho_s}{\Omega_{21}}+\frac{m_{s1}}{\Omega_{s1}}\right)\\&-\mathcal{L}_1\left(\xi_1^0,j_1+m_{s1}-1,\frac{m_{21}\phi_5^0\rho_s}{\Omega_{21}}+\frac{m_{s1}}{\Omega_{s1}}\right)\Bigg)\\&-\Delta_{j_2}^0\Bigg(\mathcal{L}_1\left(\phi_3,j_2+m_{s1}-1,\frac{m_{21}\rho_s\phi_7^0}{\Omega_{21}\varphi_{x_1'}}+\frac{m_{s1}}{\Omega_{s1}}\right)\\&-\mathcal{L}_1\left(\xi_1^0,j_2+m_{s1}-1,\frac{m_{21}\rho_s\phi_7^0}{\Omega_{21}\varphi_{x_1'}}+\frac{m_{s1}}{\Omega_{s1}}\right)\Bigg)\Bigg\}\\&\times F_{\lambda_{s2}}\left(\phi_3\right)\delta\left(\phi_7^0-\varphi_{x_1'}\phi_5^0\right),\end{aligned} \tag{34a}$$

$$\begin{aligned}\mathbb{P}_{1,1}^{t_2,x_1'}=&\mathbb{P}_{1,0}^{t_2,x_1'}\left(\xi_1^0\to\xi_1^1,\phi_7^0\to\phi_7^1,\phi_5^0\to\phi_5^1\right)\\&\times\frac{\left(1-F_{\lambda_{s2}}\left(\phi_3\right)\right)}{F_{\lambda_{s2}}\left(\phi_3\right)},\end{aligned} \tag{34b}$$

$$\begin{aligned}\mathbb{P}_{1,2}^{t_2,x_1'}=&\Bigg\{\Delta_{j_1}^2\mathcal{L}_2\left(\xi_2^2,m_{s1}+j_1-1,\frac{m_{21}\rho_s\phi_5^2}{\Omega_{21}}+\frac{m_{s1}}{\Omega_{s1}}\right)\\&-\Delta_{j_2}^2\mathcal{L}_2\left(\xi_2^2,m_{s1}+j_2-1,\frac{m_{21}\rho_s}{\Omega_{21}}\frac{\phi_7^2}{\varphi_{x_1'}}+\frac{m_{s1}}{\Omega_{s1}}\right)\Bigg\}\\&\times F_{\lambda_{s2}}\left(\phi_3\right)\delta\left(\phi_7^2-\varphi_{x_1'}\phi_5^2\right),\end{aligned} \tag{34c}$$

$$\begin{aligned}\mathbb{P}_{1,3}^{t_2,x_1'}=&\mathbb{P}_{1,2}^{t_2,x_1'}\left(\xi_2^2\to\xi_2^3,\phi_5^2\to\phi_5^3,\phi_7^2\to\phi_7^3\right)\\&\times\frac{\left(1-F_{\lambda_{s2}}\left(\phi_3\right)\right)}{F_{\lambda_{s2}}\left(\phi_3\right)},\end{aligned} \tag{34d}$$

where

$$\phi_7^A=\frac{1}{(\kappa_{1,1}^{t_2,A}b_1^A+b_2^A+\varpi^Ab_3^A)\alpha\rho_s}, \tag{35a}$$

$$\xi_1^A=\min\left\{\frac{\left(\phi_5^A+\phi_7^A\right)\varphi_{x_1'}}{(\phi_7^A-\varphi_{x_1'}\phi_5^A)\rho_s},\phi_3\right\}, \tag{35b}$$

$$\xi_2^A=\max\left\{\frac{(\phi_5^A+\phi_7^A)\varphi_{x_1'}}{(\phi_7^A-\varphi_{x_1'}\phi_5^A)\rho_s},\phi_3\right\}, \tag{35c}$$

$$\begin{aligned}\Delta_{j_1}^A=&\frac{{m_{s1}}^{m_{s1}}}{{\Omega_{s1}}^{m_{s1}}\Gamma(m_{s1})}\exp\left(-\frac{m_{21}\phi_5^A}{\Omega_{21}}\right)\\&\times\sum\nolimits_{j=0}^{m_{21}-1}\sum\nolimits_{j_1=0}^{j}\binom{j}{j_1}\left(\frac{m_{21}\phi_5^A}{\Omega_{21}}\right)^j\frac{(\rho_s)^{j_1}}{j!},\end{aligned} \tag{35d}$$

$$\begin{aligned}\Delta_{j_2}^A=&\sum\nolimits_{j=0}^{m_{21}-1}\sum\nolimits_{j_2=0}^{j}\binom{j}{j_2}\left(\frac{m_{21}\phi_7^A}{\Omega_{21}}\right)^j\left(\frac{\rho_s}{\varphi_{x_1'}}\right)^{j_2}/j!\\&\times(-1)^{j-j_2}\frac{{m_{s1}}^{m_{s1}}}{{\Omega_{s1}}^{m_{s1}}\Gamma(m_{s1})}\exp\left(\frac{m_{21}\phi_7^A}{\Omega_{21}}\right),\end{aligned} \tag{35e}$$

and the values of the step function $\delta(z)$ are zero and one for $z \le 0$ and $z > 0$, respectively.

*Proof:* See Appendix A. ■

The outage probability for $U_3$ to decode $x_{d_3}$ in the second phase should be discussed in four cases (i.e., $A = 0, 1, 2, 3$), and the corresponding expression can be written as

$$P_{3,\mathrm{out}}^{t_2,x_{d_3}} = 1 - \sum\nolimits_{\bar{k}=0}^{3} \mathbb{P}_{3,\bar{k}}^{t_2,x_{d_3}}, \tag{36}$$

where $\mathbb{P}_{3,\bar{k}}^{t_2,x_{d_3}} = \Pr(A = \bar{k}) \Pr(E_{3,x_{d_1}}^{t_2,\bar{k}} \cap E_{3,x_{d_3}}^{t_2,\bar{k}} | A = \bar{k})$.

When the events that both $U_1$ and $U_2$ cannot decode $x_3$ in the first phase occur (i.e., $A = 0$), we can use $\gamma_{1,x_3}^{t_1}$, $\gamma_{2,x_3}^{t_1}$, $\gamma_{3,x_{d_1}}^{t_2,0}$ and $\gamma_{3,x_{d_3}}^{t_2,0}$ to calculate $\mathbb{P}_{3,0}^{t_2,x_{d_3}}$ as

$$\begin{aligned}\mathbb{P}_{3,0}^{t_2,x_{d_3}} &= \Pr\left(\lambda_{s1} < \phi_3, \lambda_{s2} < \phi_3, \lambda_{23} > \tilde{\phi}_4^0\right) \\ &= F_{\lambda_{s1}}(\phi_3) F_{\lambda_{s2}}(\phi_3)\left(1 - F_{\lambda_{23}}\left(\tilde{\phi}_4^0\right)\right),\end{aligned} \tag{37}$$

where $\tilde{\phi}_4^A = \max\left\{\phi_4^A, \phi_8^A\right\}$ and $\phi_8^A = \frac{\varphi_{x_{d_3}}}{\alpha\rho_s\left(b_2^A - \left(\kappa_{3,2}^{t_2,A} b_1^A + \kappa_{3,3}^{t_2,A} b_3^A\right)\varphi_{x_{d_3}}\right)}$. Similarly, the condition $\phi_8^A > 0$ should be met, otherwise the outage probability for $U_3$ to decode $x_{d_3}$ is always one.

If $U_1$ cannot decode $x_3$ in the first phase while $U_2$ can decode $x_3$ successfully (i.e., $A = 1$), the non-outage probability for $U_3$ to decode $x_{d_3}$ during the second phase can be calculated as

$$\begin{aligned}\mathbb{P}_{3,1}^{t_2,x_{d_3}} &= \Pr\left(\lambda_{s1} < \phi_3, \lambda_{s2} > \phi_3, \lambda_{23} > \tilde{\phi}_5^1\right) \\ &= F_{\lambda_{s1}}(\phi_3)\left(1 - F_{\lambda_{s2}}(\phi_3)\right)\left(1 - F_{\lambda_{23}}\left(\tilde{\phi}_5^1\right)\right),\end{aligned} \tag{38}$$

where $\tilde{\phi}_5^A = \max\left\{\phi_4^A, \phi_6^A, \phi_8^A\right\}$.

Similar to (37), using $\gamma_{1,x_3}^{t_1}$, $\gamma_{2,x_3}^{t_1}$, $\gamma_{3,x_{d_1}}^{t_2,2}$ and $\gamma_{3,x_{d_3}}^{t_2,2}$, we can calculate $\mathbb{P}_{1,2}^{t_2,x_{d_3}}$ as

$$\begin{aligned}\mathbb{P}_{3,2}^{t_2,x_{d_3}} &= \Pr\left(\lambda_{s1} > \phi_3, \lambda_{s2} < \phi_3, \lambda_{23} > \tilde{\phi}_4^2\right) \\ &= \left(1 - F_{\lambda_{s1}}(\phi_3)\right) F_{\lambda_{s2}}(\phi_3)\left(1 - F_{\lambda_{23}}\left(\tilde{\phi}_4^2\right)\right).\end{aligned} \tag{39}$$

When the events that both $U_1$ and $U_2$ can decode $x_3$ successfully during the second phase occur (i.e., $A = 3$), the non-outage probability for $U_3$ to decode $x_{d_3}$ can be calculated by using $\gamma_{1,x_3}^{t_1}$, $\gamma_{2,x_3}^{t_1}$, $\gamma_{3,x_{d_1}}^{t_2,3}$, $\gamma_{3,x_3}^{t_2,3}$ and $\gamma_{3,x_{d_3}}^{t_2,3}$ as

$$\begin{aligned}\mathbb{P}_{3,3}^{t_2,x_{d_3}} &= \Pr\left(\lambda_{s1} > \phi_3, \lambda_{s2} > \phi_3, \lambda_{23} > \tilde{\phi}_5^3\right) \\ &= \left(1 - F_{\lambda_{s1}}(\phi_3)\right)\left(1 - F_{\lambda_{s2}}(\phi_3)\right) \\ &\quad \times \left(1 - F_{\lambda_{23}}\left(\tilde{\phi}_5^3\right)\right).\end{aligned} \tag{40}$$

Substituting (37), (38), (39) and (40) into (36), we obtain $P_{3,\mathrm{out}}^{t_2,x_{d_3}}$.

Based on the derivations of the outage probability, the following theorem provides the diversity orders of all the data streams to investigate the diversity gain of the proposed scheme.

*Theorem 2:* The achievable diversity orders achieved by the data streams $x_1$, $x_2$, $x_3$, $x_1'$, $x_{d_1}$ and $x_{d_3}$ are one, one, one, zero, zero and one, respectively.

*Proof:* See Appendix B. ■

Furthermore. using (19), (21), (22), (25), (33) and (36), we can write the outage throughput for the proposed scheme as

$$\begin{aligned}\mathcal{T} = &\left(1 - P_{1,\mathrm{out}}^{t_1,x_1}\right) R_{x_1} + \left(1 - P_{2,\mathrm{out}}^{t_1,x_2}\right) R_{x_2} \\ &+ \left(1 - P_{3,\mathrm{out}}^{t_2,x_3}\right) R_{x_3} + \left(1 - P_{1,\mathrm{out}}^{t_2,x_{d_1}}\right) R_{x_{d_1}} \\ &+ \left(1 - P_{1,\mathrm{out}}^{t_2,x_1'}\right) R_{x_1'} + \left(1 - P_{3,\mathrm{out}}^{t_2,x_{d_3}}\right) R_{x_{d_3}}.\end{aligned} \tag{41}$$

## *B. Ergodic Sum Capacity and Average SE*

When the target data rates vary dynamically according to the channel qualities, the ergodic sum capacity for the proposed scheme can be expressed as

$$\bar{C}_{\mathrm{sum}} = \sum\nolimits_{\forall \dot{x} \in \dot{X}} \bar{C}_{\dot{x}} + \sum\nolimits_{\forall \ddot{x} \in \ddot{X}} \bar{C}_{\ddot{x}}^3, \tag{42}$$

where $\bar{C}_{\dot{x}} = \mathbb{E}[C_{\dot{x}}]$, $\bar{C}_{\ddot{x}}^3 = \mathbb{E}[C_{\ddot{x}}^3]$, $\dot{X} \in \{x_1, x_2\}$ and $\ddot{X} \in \{x_3, x_{d_1}, x_{d_3}, x_1'\}$.

For simplicity, we first provide some defined functions and integral calculation equations before deriving the ergodic capacity. Applying [39, eq.(3.353.5)] to the following integral, we have

$$\begin{aligned}\mathcal{L}_3(\eta, \mu) &\triangleq \int_0^\infty \frac{z^\eta}{1+z} \exp(-\mu z) dz \\ &= \sum\nolimits_{\kappa=1}^{\eta} (-1)^{\eta-\kappa} (\kappa - 1)! \mu^{-\kappa} \\ &\quad + (-1)^{\eta-1} \exp(\mu) \mathrm{Ei}(-\mu),\end{aligned} \tag{43}$$

where $\mathrm{Ei}(\cdot)$ is the exponential integral function. Using the variable substitution, binomial expansion and [39, eqs.(3.351.2) and (3.351.4)], we can define the following integral as

$$\begin{aligned}&\mathcal{L}_4(\eta, \bar{\eta}, \eta^*, \mu) \triangleq \int_0^\infty \frac{z^\eta}{(z + \eta^*)^{\bar{\eta}}} \exp(-\mu z) dz \\ &= \sum\nolimits_{\eta_1=0}^{\eta} \binom{\eta}{\eta_1} (-\eta^*)^{\eta-\eta_1} \exp(\mu\eta^*) \\ &\times \begin{cases} \exp(-\mu\eta^*) \sum_{\eta_2=0}^{\eta_1-\bar{\eta}} \frac{(\eta_1-\bar{\eta})!(\eta^*)^{\eta_2}}{\eta_2! \mu^{\eta_1-\bar{\eta}-\eta_2+1}}, & \eta_1 - \bar{\eta} \ge 0, \\ \frac{-(-\mu)^{\bar{\eta}-\eta_1-1} \mathrm{Ei}(-\mu\eta^*)}{(\bar{\eta}-\eta_1-1)!} + \frac{\exp(-\mu\eta^*)}{(\eta^*)^{\bar{\eta}-\eta_1-1}} & \\ \times \sum_{\eta_3=0}^{\bar{\eta}-\eta_1-2} \frac{(-\mu\eta^*)^{\eta_3} (\bar{\eta}-\eta_1-\eta_3-2)!}{(\bar{\eta}-\eta_1-1)!}, & \eta_1 - \bar{\eta} < 0, \end{cases}\end{aligned} \tag{44}$$

where $\eta^*$ denotes a constant. Moreover, we give an integral calculation equation

$$\int_0^\infty \ln(z+1) f_Z(z) dz = \int_0^\infty \frac{1 - F_Z(z)}{1+z} dz. \tag{45}$$

Let $X_1 \triangleq \lambda_{s1}(a_1 + \kappa_{1,2}^{t_1} a_2 + \kappa_{1,3}^{t_1} a_3)\rho_s$ and $X_2 \triangleq \lambda_{s1}(\kappa_{1,2}^{t_1} a_2 + \kappa_{1,3}^{t_1} a_3)\rho_s$. Using (4), (13) and (45), we have

$$\begin{aligned}\bar{C}_{x_1} = &\frac{1}{2\ln 2}\left\{\int_0^\infty \frac{1 - F_{X_1}(x)}{1+x} dx - \int_0^\infty \frac{1 - F_{X_2}(x)}{1+x} dx\right\} \\ = &\frac{1}{2\ln 2}\left\{\Delta_{d_1} \mathcal{L}_3\left(d_1, \frac{m_{s1}}{\Omega_{s1}\left(a_1 + \kappa_{1,2}^{t_1} a_2 + \kappa_{1,3}^{t_1} a_3\right)\rho_s}\right)\right. \\ &\left. - \Delta_{d_2} \mathcal{L}_3\left(d_2, \frac{m_{s1}}{\Omega_{s1}\left(\kappa_{1,2}^{t_1} a_2 + \kappa_{1,3}^{t_1} a_3\right)\rho_s}\right)\right\},\end{aligned} \tag{46}$$

where $\Delta_{d_1} = \sum_{d_1=0}^{m_{s1}-1} \left(\frac{m_{s1}}{\Omega_{s1}\left(a_1 + \kappa_{1,2}^{t_1} a_2 + \kappa_{1,3}^{t_1} a_3\right)\rho_s}\right)^{d_1} / d_1!$, $\Delta_{d_2} = \sum_{d_2=0}^{m_{s1}-1} \left(\frac{m_{s1}}{\Omega_{s1}\left(\kappa_{1,2}^{t_1} a_2 + \kappa_{1,3}^{t_1} a_3\right)\rho_s}\right)^{d_2} / d_2!$,

This article has been accepted for publication in a future issue of this journal, but has not been fully edited. Content may change prior to final publication. Citation information: DOI 10.1109/JSAC.2022.3143267, IEEE Journal on Selected Areas in Communications



$F_{X_1}(x) = F_{\lambda_{s1}}\left(\frac{x}{(a_1+\kappa_{1,2}^{t_1}a_2+\kappa_{1,3}^{t_1}a_3)\rho_s}\right)$ and $F_{X_2}(x) = F_{\lambda_{s1}}\left(\frac{x}{(\kappa_{1,2}^{t_1}a_2+\kappa_{1,3}^{t_1}a_3)\rho_s}\right)$. Note that the equation $\mathcal{L}_3(\eta,\infty)=0$ holds.

For mathematical tractability, we assume that $U_1$ and $U_2$ suffer the same residual interference as $x_3$ (i.e., $\kappa_{1,1}^{t_1}=\kappa_{2,1}^{t_1}$) when $U_1$ and $U_2$ perform imperfect SIC to decode $x_3$ in the first phase. Let $Y \triangleq \min(\lambda_{s1},\lambda_{s2})$, $Y_1 \triangleq Y(a_1+a_2+\kappa_{1,1}^{t_1}a_3)\rho_s$ and $Y_2 \triangleq Y(a_1+\kappa_{1,1}^{t_1}a_3)\rho_s$. Using the order statistic, we can obtain the CDF of $Y$ as

$$\begin{aligned}F_Y(y) &= 1-(1-F_{\lambda_{s1}}(y))(1-F_{\lambda_{s2}}(y))\\ &=1-\Delta_e y^{e_1+e_2}\exp\left(-\left(\frac{m_{s1}}{\Omega_{s1}}+\frac{m_{s2}}{\Omega_{s2}}\right)y\right),\end{aligned} \quad (47)$$

where $\Delta_e = \sum_{e_1=0}^{m_{s1}-1}\sum_{e_2=0}^{m_{s2}-1}\left(\frac{m_{s1}}{\Omega_{s1}}\right)^{e_1}\left(\frac{m_{s2}}{\Omega_{s2}}\right)^{e_2}/e_1!/e_2!$. Furthermore, the CDFs of $Y_1$ and $Y_2$ can be written as $F_{Y_1}(y) = F_Y\left(\frac{y}{(a_1+a_2+\kappa_{1,1}^{t_1}a_3)\rho_s}\right)$ and $F_{Y_2}(y) = F_Y\left(\frac{y}{(a_1+\kappa_{1,1}^{t_1}a_3)\rho_s}\right)$, respectively. Using (3), (16), (45) and (47), we can calculate $\bar{C}_{x_2}$ as

$$\begin{aligned}\bar{C}_{x_2} &= \frac{1}{2\ln 2}\left\{\int_0^\infty \frac{1-F_{Y_1}(y)}{1+y}dy - \int_0^\infty \frac{1-F_{Y_2}(y)}{1+y}dy\right\}\\ &= \frac{1}{2\ln 2}\left\{\Delta_{e_1}\mathcal{L}_3(e_1+e_2,\Theta_1) - \Delta_{e_2}\mathcal{L}_3(e_1+e_2,\Theta_2)\right\},\end{aligned} \quad (48)$$

where $\Delta_{e_1} = \Delta_e\left(\left(a_1+a_2+\kappa_{1,1}^{t_1}a_3\right)\rho_s\right)^{-e_1-e_2}$, $\Delta_{e_2} = \Delta_e\left(\left(a_1+\kappa_{1,1}^{t_1}a_3\right)\rho_s\right)^{-e_1-e_2}$, $\Theta_1 = \frac{m_{s1}/\Omega_{s1}+m_{s2}/\Omega_{s2}}{(a_1+a_2+\kappa_{1,1}^{t_1}a_3)\rho_s}$ and $\Theta_2 = \frac{m_{s1}/\Omega_{s1}+m_{s2}/\Omega_{s2}}{(a_1+\kappa_{1,1}^{t_1}a_3)\rho_s}$.

The ergodic capacity of $x_3$ is determined by $\bar{U} \triangleq \min\{\bar{U}_1,\bar{U}_2,\bar{U}_3\}$, where $\bar{U}_1 \triangleq \gamma_{1,x_3}^{t_1}$, $\bar{U}_2 \triangleq \gamma_{2,x_3}^{t_1}$ and $\bar{U}_3 \triangleq \gamma_{3,x_3}^{t_2,3}$. The CDF of $\bar{U}_i$, $i\in\{1,2,3\}$ is given by

$$F_{\bar{U}_i}(u) = \begin{cases} \bar{F}_{\bar{U}_i}(u), & u<\theta_i,\\ 1, & u\geq\theta_i,\end{cases} \quad (49)$$

where $\bar{F}_{\bar{U}_1}(u) = F_{\lambda_{s1}}\left(\frac{u}{(a_3-(a_1+a_2)u)\rho_s}\right)$, $\bar{F}_{\bar{U}_2}(u) = F_{\lambda_{s2}}\left(\frac{u}{(a_3-(a_1+a_2)u)\rho_s}\right)$, $\bar{F}_{\bar{U}_3}(u) = F_{\lambda_{23}}\left(\frac{u}{(b_3^3-(\kappa_{3,1}^{t_2,3}b_1^3+b_2^3)u)\alpha\rho_s}\right)$, $\theta_1=\theta_2=\frac{a_3}{a_1+a_2}$ and $\theta_3=\frac{b_3^3}{\kappa_{3,1}^{t_2,3}b_1^3+b_2}$. Using (49) and order statistic, we have

$$\begin{aligned}F_{\bar{U}}(u) &= 1-\Pi_{i=1}^3(1-F_{\bar{U}_i}(u))\\ &= \begin{cases}1-\Pi_{i=1}^3(1-\bar{F}_{\bar{U}_i}(u)), & u<\tilde{\theta},\\ 1, & u\geq\tilde{\theta},\end{cases}\end{aligned} \quad (50)$$

where $\tilde{\theta}=\min\{\theta_1,\theta_3\}$. Based on (18), (45) and (50), we can use Gaussian-Chebyshev quadrature to approximate $\bar{C}_{x_3}^3$ as

$$\begin{aligned}\bar{C}_{x_3}^3 &= \frac{1}{2\ln 2}\int_0^{\tilde{\theta}} \frac{\Pi_{i=1}^3\left(1-\bar{F}_{\bar{U}_i}(u)\right)}{1+u}du\\ &\approx \frac{\tilde{\theta}\pi}{4\ln 2}\sum_{n_1=1}^{N_1}\frac{\sqrt{1-\psi_{n_1}^2}}{N_1}\frac{\Pi_{i=1}^3\left(1-\bar{F}_{\bar{U}_i}(q_{n_1})\right)}{1+q_{n_1}},\end{aligned} \quad (51)$$

where $q_{n_1} = \frac{(1+\psi_{n_1})\tilde{\theta}}{2}$, $\psi_{n_1} = \cos\left(\frac{2n_1-1}{2N_1}\pi\right)$, and $N_1$ is a complexity-accuracy tradeoff parameter.

Let $V \triangleq \gamma_{1,x_1'}^{t_2,3}$. The CDF of $V$ can be written as $F_V(v) = 1-\Delta_f(v+F_1)^{-f_1-m_{21}}v^f\exp\left(-\frac{m_{s1}}{\Omega_{s1}\rho_s}v\right)$ by using (9), (20) and the binomial expansion, where $\Delta_f = \frac{m_{21}{}^{m_{21}}}{\Omega_{21}{}^{m_{21}}\Gamma(m_{21})}\sum_{f=0}^{m_{s1}-1}\sum_{f_1=0}^{f}\binom{f}{f_1}\frac{(f_1+m_{21}-1)!}{f!}\left(\frac{m_{s1}}{\Omega_{s1}}\right)^{f-f_1-m_{21}} \times \left(\kappa_{1,1}^{t_2,3}b_1^3+b_2^3\right)^{-m_{21}}\alpha^{-m_{21}}\rho_s{}^{f_1-f}$ and $F_1 = \frac{m_{21}\Omega_{s1}}{m_{s1}\Omega_{21}\left(\kappa_{1,1}^{t_2,3}b_1^3+b_2^3\right)\alpha}$. Thus, using (14), (45), (46), (47), and the partial fraction decomposition, we can calculate the closed-form expression of $\bar{C}_{x_1'}^3$ as

$$\begin{aligned}\bar{C}_{x_1'}^3 &= \frac{\Delta_f}{2\ln 2}\int_0^\infty \frac{v^f}{(v+F_1)^{f_1+m_{21}}(1+v)}\exp\left(-\frac{m_{s1}}{\Omega_{s1}\rho_s}v\right)dv\\ &= \frac{\Delta_f}{2\ln 2}\left\{\sum_{f_2=1}^{f_1+m_{21}} - \frac{1}{(F_1-1)^{f_2}}\mathcal{L}_4\left(f,\bar{f},F_1,\frac{m_{s1}}{\Omega_{s1}\rho_s}\right)\right.\\ &\quad\left.+\frac{1}{(F_1-1)^{f_1+m_{21}}}\mathcal{L}_3\left(f,\frac{m_{s1}}{\Omega_{s1}\rho_s}\right)\right\},\end{aligned} \quad (52)$$

where $\bar{f} = f_1+m_{21}-f_2+1$.

Let $W_1 \triangleq \gamma_{3,x_{d1}}^{t_2,3}$, $W_2 \triangleq \gamma_{1,x_{d1}}^{t_2,3}$ and $W \triangleq \min\{W_1,W_2\}$. Similar to (50), the CDF of $W$ can be expressed as

$$\begin{aligned}F_W(w) &= 1-\Pi_{i=1}^2(1-F_{W_i}(w))\\ &= \begin{cases}1-\Pi_{i=1}^2(1-\bar{F}_{W_i}(w)), & w<\frac{b_1^3}{b_2^3+b_3^3},\\ 1, & w\geq\frac{b_1^3}{b_2^3+b_3^3},\end{cases}\end{aligned} \quad (53)$$

where $\bar{F}_{W_1}(w) = F_{\lambda_{23}}\left(\frac{w}{\alpha\rho_s(b_1^3-(b_2^3+b_3^3)w)}\right)$, $\bar{F}_{W_2}(w) = 1-\Delta_g(w)G(w)^{-g_1-m_{s1}}$, $G(w) = \frac{m_{21}\rho_s w}{(b_1^3-b_2^3w)\alpha\rho_s\Omega_{21}}+\frac{m_{s1}}{\Omega_{s1}}$, $\Delta_g(w) = \sum_{g=0}^{m_{21}-1}\sum_{g_1=0}^{g}\frac{m_{s1}{}^{m_{s1}}}{\Omega_{s1}{}^{m_{s1}}\Gamma(m_{s1})g!}\left(\frac{m_{21}}{\Omega_{21}}\right)^g\binom{g}{g_1}\rho_s{}^{g_1}(g_1+m_{s1}-1)!\left(\frac{w}{(b_1^3-b_2^3w)\alpha\rho_s}\right)^g\exp\left(-\frac{m_{21}w}{(b_1^3-b_2^3w)\alpha\rho_s\Omega_{21}}\right)$. Therefore, we can use (17), (45), (53), and Gaussian-Chebyshev quadrature to obtain an approximation of $\bar{C}_{x_{d_1}}^3$ as

$$\begin{aligned}\bar{C}_{x_{d_1}}^3 \approx& \frac{b_1^3\pi}{4(b_2^3+b_3^3)\ln 2}\sum_{n_2=1}^{N_2}\frac{\sqrt{1-\psi_{n_2}^2}}{N_2}\\ &\times\frac{\Pi_{i=1}^2(1-\bar{F}_{W_i}(q_{n_2}))}{1+q_{n_2}},\end{aligned} \quad (54)$$

where $q_{n_2} = \frac{(1+\psi_{n_2})b_1^3}{2(b_2^3+b_3^3)}$, $\psi_{n_2} = \cos\left(\frac{2n_2-1}{2N_2}\pi\right)$, $N_2$ denotes a complexity-accuracy tradeoff parameter.

Following the same steps in (46), we can use $\gamma_{3,x_{d_3}}^{t_2,3}$ to calculate $\bar{C}_{x_{d_3}}^3$ as

$$\begin{aligned}\bar{C}_{x_{d_3}}^3 =& \frac{1}{2\ln 2}\left\{\Delta_{h_1}\mathcal{L}_3\left(h_1,\frac{m_{23}}{\Omega_{23}\left(b_2^3+\kappa_{3,2}^{t_2,3}b_1^3+\kappa_{3,3}^{t_2,3}b_3^3\right)\alpha\rho_s}\right)\right.\\ &\left.-\Delta_{h_2}\mathcal{L}_3\left(h_2,\frac{m_{23}}{\Omega_{23}\left(\kappa_{3,2}^{t_2,3}b_1^3+\kappa_{3,3}^{t_2,3}b_3^3\right)\alpha\rho_s}\right)\right\},\end{aligned} \quad (55)$$

where $\Delta_{h_1} = \sum_{h_1=0}^{m_{23}-1}\left(\frac{m_{23}}{\Omega_{23}(b_2^3+\kappa_{3,2}^{t_2,3}b_1^3+\kappa_{3,3}^{t_2,3}b_3^3)\alpha\rho_s}\right)^{h_1}/h_1!$ and $\Delta_{h_2} = \sum_{h_2=0}^{m_{23}-1}\left(\frac{m_{23}}{\Omega_{23}(\kappa_{3,2}^{t_2,3}b_1^3+\kappa_{3,3}^{t_2,3}b_3^3)\alpha\rho_s}\right)^{h_2}/h_2!$.

Combining (42), (46), (48), (51), (52), (54) and (55), we obtain $\bar{C}_{\mathrm{sum}}$.

Based on [40, eq.(3.104)] and (42), the average SE can be defined as the average number of delivered bits per bandwidth

$$\bar{C}_{\mathrm{SE}} \triangleq \frac{\bar{C}_{\mathrm{sum}}}{W_B}, \tag{56}$$

where $W_B$ represents the occupied bandwidth. To analyze the average SE of the proposed scheme, we consider the unit time (i.e., 1 s) and normalized bandwidth (i.e., $W_B = 1$ Hz) in this paper. Therefore, using the previous analysis of the ergodic sum capacity, we obtain $\bar{C}_{\mathrm{SE}} = \bar{C}_{\mathrm{sum}}$.

The following theorem gives the SE scaling of the proposed scheme to achieve more insights into the average SE.

*Theorem 3:* In the high transmit SNR region (i.e., $\rho_s \rightarrow \infty$), the SE scaling of the proposed scheme with perfect and imperfect SIC are $\log_2 \rho_s$ and zero, respectively.

*Proof:* See Appendix C. ∎

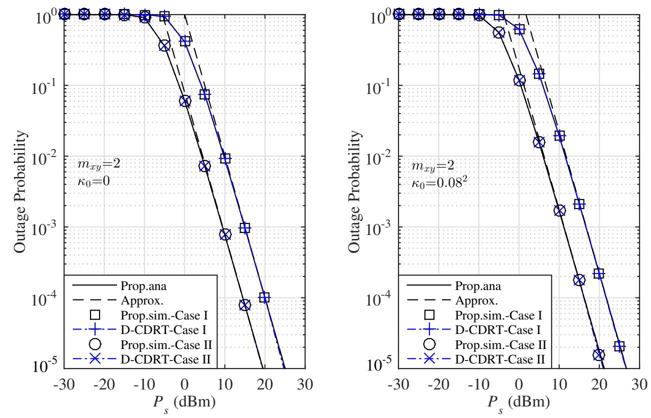


(a) Perfect SIC (b) Imperfect SIC

Fig. 2. Outage probability for $U_1$ to decode $x_1$ in $t_1$ (i.e., $P_{1,\mathrm{out}}^{t_1,x_1}$).

## V. Numerical Results

In this section, we adopt extensive Monte Carlo simulations to investigate the performance of the proposed adaptive transmission scheme with both perfect and imperfect SIC. Specifically, the outage probability, outage throughput and average SE of the proposed scheme (Prop.) are compared with the conventional D-CDRT scheme in [34] using the same simulation parameters. In the simulations, we consider two distance settings, i.e., Case I: $d_{s1} = 80$ m, $d_{s2} = 90$ m, $d_{21} = 15$ m, and $d_{23} = 5$ m; Case II: $d_{s1} = 50$ m, $d_{s2} = 55$ m, $d_{21} = 10$ m, and $d_{23} = 5$ m. The channel gain for reference distance, the path loss exponent, the noise power, and the scale factor are set to $G_0 = -40$ dB, $\alpha_0 = 2.7$, $N_0 = -110$ dBm, and $\alpha = 0.05$, respectively. Moreover, the target data rates are set to $R_{x_1} = R_{x_2} = R_{x_3} = R_{x_{d_3}} = 0.3$ bit/s/Hz and $R'_{x_1} = R_{x_{d_1}} = 0.1$ bit/s/Hz. The power allocation coefficients are $a_1 = 0.01$, $a_2 = 0.09$ and $a_3 = 0.9$, and the power allocation coefficient combinations ($A$, $b_1^A$, $b_2^A$, $b_3^A$) are set to (0, 0.99, 0.01, 0), (1, 0.9, 0.01, 0.09), (2, 0.99, 0.01, 0) and (3, 0.9, 0.01, 0.09). For simplicity, we assumed that all the fractional error factors (e.g., $\kappa_{1,2}^{t_1}$ and $\kappa_{1,1}^{t_2,A}$) equal $\kappa_0$ for imperfect SIC [41].

To implement NOMA successfully, the conventional D-CDRT scheme requires power control at BS. Since $d_{s1} < d_{s2}$ and $d_{23} < d_{21}$, the power allocation coefficients of the D-CDRT are set as $\alpha_{e1} = a_2 + a_3$, $\alpha_c = a_1$, $\alpha_d = b_1^3 + b_3^3$ and $\alpha_{e2} = b_2^3$, while the corresponding power ratio is assumed to be $\beta = \frac{\alpha_d P_u}{2P_s}$ for fair comparisons.

### *A. Outage Probability and Outage Throughput*

In Fig. 2, we plot the outage probability for $U_1$ to decode $x_1$ in $t_1$ ($P_{1,\mathrm{out}}^{t_1,x_1}$) versus the transmit power of BS with both perfect SIC and imperfect SIC. Fig. 2 validates that the accurate theoretical results for the proposed scheme are in good agreement with the simulation ones. Fig. 2 illustrates that the proposed scheme achieves the same outage probability for $U_1$ in $t_1$ as the conventional D-CDRT scheme. This is because the decoding procedure and parameter settings (i.e., the target data rates, power allocation coefficients and fractional error factors) of the proposed scheme are consistent with the conventional one. Although the decoding process of $x_1$ is affected by the residual interference caused by imperfect SIC, this process will not face the adjacent-channel interference. Therefore, the outage probability corresponding to $x_1$ becomes large with the increase of the residual interference level, while it has no error floors for large $P_s$. Meanwhile, the asymptotic lines are well-matched for the corresponding theoretical lines in the high transmit SNR region, which verifies the correctness of the approximate result and diversity order analysis in Theorem 2.

Fig. 3 compares the outage probability for $U_3$ to decode $x_3$ in $t_2$ (i.e., $P_{3,\mathrm{out}}^{t_2,x_3}$) of the proposed scheme and the conventional D-CDRT scheme. From Fig. 3, the simulations of the proposed scheme agree well with the corresponding theoretical results, and the asymptotic lines gradually coincide with the theoretical ones when $P_s$ increases. Unlike the stationary transmission scheme of the conventional D-CDRT scheme, the proposed scheme designs an adaptive aggregate transmission and a pre-determined decoding order strategy, and thus $U_3$ can receive $x_3$ in $t_2$ as long as $U_2$ can decode $x_3$ successfully in $t_1$. Based on this, the proposed scheme can achieve a lower $P_{3,\mathrm{out}}^{t_2,x_3}$ than that of the conventional D-CDRT scheme with perfect and imperfect SIC, and the performance superiority becomes more evident in Case II. The proposed scheme has better robustness for facing imperfect SIC than that of the conventional D-CDRT scheme.

Fig. 4 shows the relationship between the outage probability for $U_1$ to decode $x'_1$ in $t_2$ (i.e., $P_{1,\mathrm{out}}^{t_2,x'_1}$) and the transmit power of BS. In this figure, the simulation results are consistent with the theoretical ones. Since $U_1$ suffers the inter-user interference from $U_2$ in $t_2$, both the proposed and conventional schemes have error floors for the outage probability related to $x'_1$ for large $P_s$. Specifically, when perfect SIC is performed, the proposed scheme has a higher error floor for large $P_s$ than the conventional scheme due to the aggregation transmission. However, the proposed scheme using the adaptive transmission can achieve better outage performance for small $P_s$. If imperfect SIC is performed, $P_{1,\mathrm{out}}^{t_2,x'_1}$ in the conventional scheme significantly decreases, while this phenomenon is not apparent in the proposed scheme because of adaptive transmission.

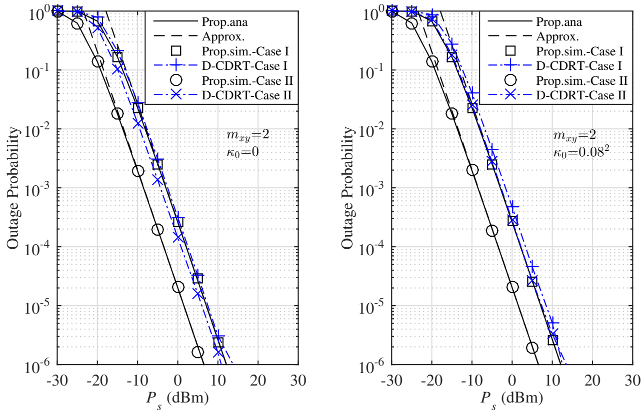


(a) Perfect SIC (b) Imperfect SIC

Fig. 3. Outage probability for $U_3$ to decode $x_3$ in $t_2$ (i.e., $P_{3,\text{out}}^{t_2,x_3}$).

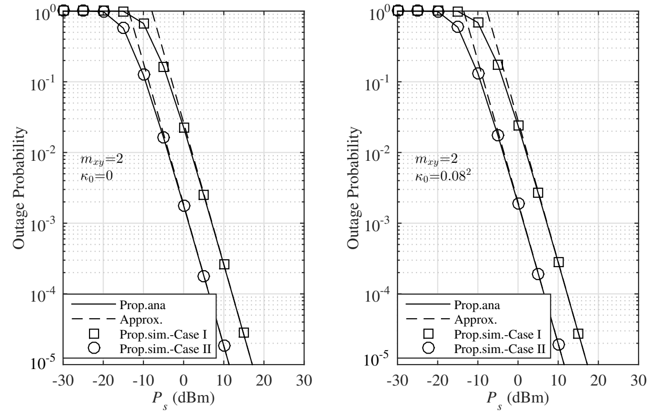


(a) Perfect SIC (b) Imperfect SIC

Fig. 6. Outage probability for $U_2$ to decode $x_2$ in $t_1$ (i.e., $P_{2,\text{out}}^{t_1,x_2}$).

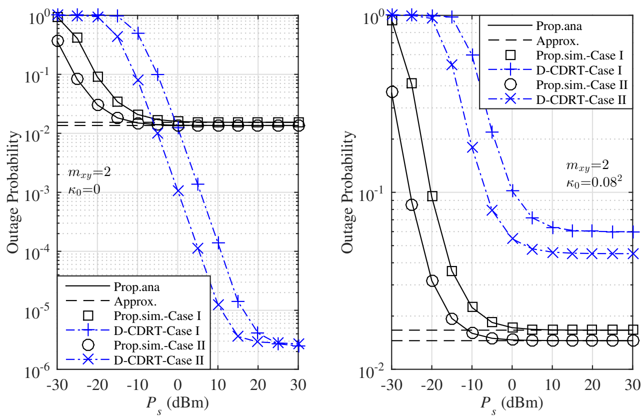


(a) Perfect SIC (b) Imperfect SIC

Fig. 4. Outage probability for $U_1$ to decode $x_1'$ in $t_2$ (i.e., $P_{1,\text{out}}^{t_2,x_1'}$).

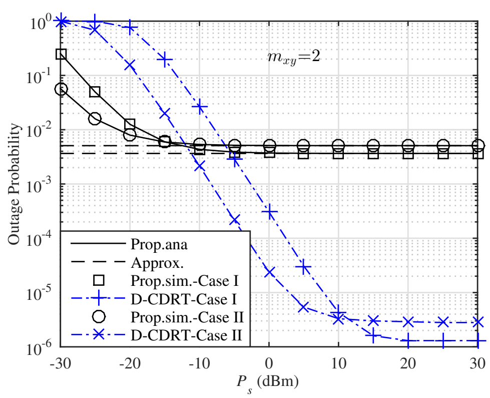


Fig. 5. Outage probability for $U_1$ to decode $x_{d_1}$ in $t_2$ (i.e., $P_{1,\text{out}}^{t_2,x_{d_1}}$).

In Fig. 5, the outage probability for $U_1$ to decode $x_{d_1}$ in $t_2$ (i.e., $P_{1,\text{out}}^{t_2,x_{d_1}}$) versus the transmit power of BS is illustrated. The simulation results of the proposed scheme agree with the corresponding theoretical results perfectly. It is worth noting that the decoding process of $x_{d_1}$ for the proposed scheme and conventional one will not suffer the residual interference, and thus imperfect SIC has no impact on $P_{1,\text{out}}^{t_2,x_{d_1}}$. Due to the interference from BS, $P_{1,\text{out}}^{t_2,x_{d_1}}$ for the proposed scheme and conventional one are subject to error floors for large $P_s$, which verifies that $P_{1,\text{out}}^{t_2,x_{d_1}}$ has the diversity order of one. Meanwhile, the asymptotic line gradually coincides with the corresponding error floor with the increase of $P_s$. The proposed scheme achieves a higher error floor of $P_{1,\text{out}}^{t_2,x_{d_1}}$ for larger $P_s$ because a portion of the transmit power at $U_2$ is allocated to $x_{d3}$. Conversely, the proposed scheme can attain lower $P_{1,\text{out}}^{t_2,x_{d_1}}$ for small $P_s$, which benefits from the design of adaptive transmission.

Fig. 6 and Fig. 7 depict the outage probabilities for $U_2$ and $U_3$ to decode $x_2$ and $x_{d_3}$ in $t_1$ and $t_2$ (i.e., $P_{2,\text{out}}^{t_1,x_2}$ and $P_{3,\text{out}}^{t_2,x_{d_3}}$), respectively. In these two figures, the correctness of the theoretical analysis for the proposed scheme is verified through simulations, and the asymptotic result is well-matched with the theoretical value. The proposed scheme can use the same amount of time resource to transmit two extra data streams (i.e., $x_2$ and $x_{d_3}$) compared with the conventional scheme. From Fig. 6, we observe that $P_{2,\text{out}}^{t_1,x_2}$ in Case II is lower than that in Case I. This is because Case II has a larger $\lambda_{s2}$ than that in Case I. As expected, $P_{2,\text{out}}^{t_1,x_2}$ becomes large as the residual interference level increases. In Fig. 7, the lines for $P_{3,\text{out}}^{t_2,x_{d_3}}$ in Case I almost coincide with that in Case II under perfect and imperfect SIC, because both Case I and Case II have the same $d_{23}$. Besides, imperfect SIC can increase $P_{3,\text{out}}^{t_2,x_{d_3}}$, which is consistent with the analysis in (36). Moreover, both $P_{2,\text{out}}^{t_1,x_2}$ and $P_{3,\text{out}}^{t_2,x_{d_3}}$ have no error floors, and they can attain the diversity order of one.

In Fig. 8, the outage throughput versus $P_s$ is illustrated under both perfect and imperfect SIC. The simulations validate the theoretical results in (41). Fig. 8 shows that the proposed scheme can attain high outage throughput than the conventional scheme. This is because the proposed scheme can use the same amount of time resource to transmit two more data streams through aggregate transmission. Meanwhile, since the outage throughput is affected by the outage probability and

This article has been accepted for publication in a future issue of this journal, but has not been fully edited. Content may change prior to final publication. Citation information: DOI 10.1109/JSAC.2022.3143267, IEEE Journal on Selected Areas in Communications



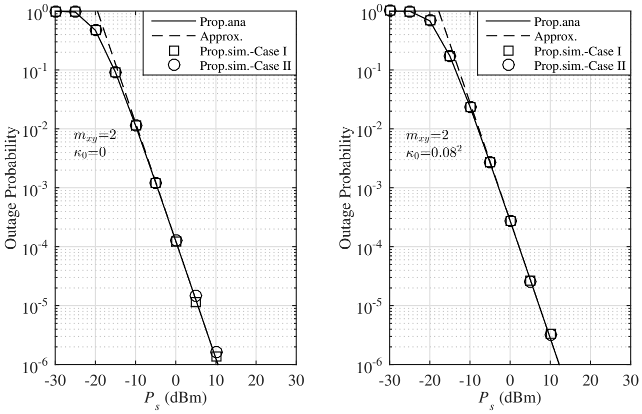


(a) Perfect SIC (b) Imperfect SIC

Fig. 7. Outage probability for $U_3$ to decode $x_{d_3}$ in $t_2$ (i.e., $P_{3,\mathrm{out}}^{t_2,x_{d_3}}$).

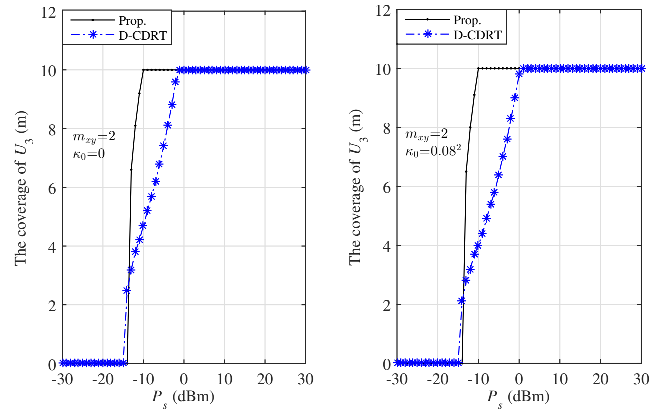


(a) Perfect SIC (b) Imperfect SIC

Fig. 9. The coverage of the CEU $U_3$ versus the transmit power of BS.

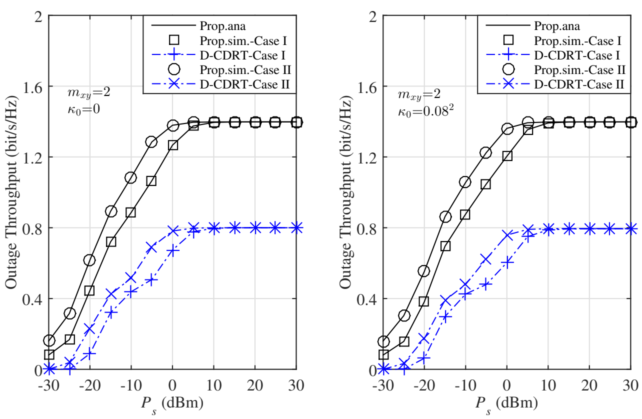


(a) Perfect SIC (b) Imperfect SIC

Fig. 8. Comparison of outage throughput between the proposed scheme and the conventional D-CDRT.

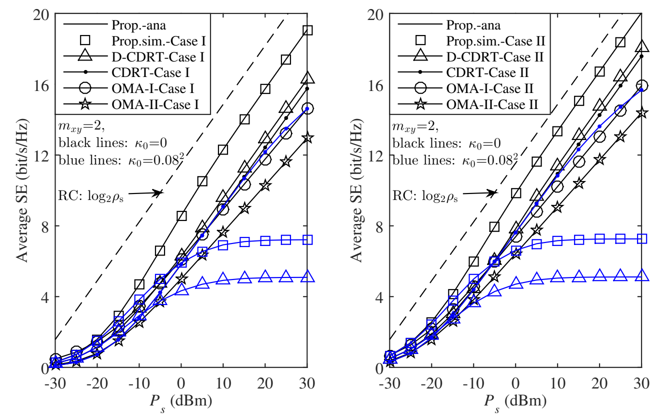


(a) Case I (b) Case II

Fig. 10. Comparison of average SE among the proposed scheme, the conventional D-CDRT, CDRT, OMA-I, and OMA-II, and RC represents the reference curve.

target data rate for large $P_s$, both the proposed and conventional schemes have the ceilings of the outage throughput. The outage throughput for Case II is better than that for Case I in the low-medium transmit power region because the channel quality of Case II is better than that of Case I. However, for large $P_s$, the outage throughput of Case II is almost the same as that of Case I. This is because the error floor determines the outage throughput, and the error floor differences between Case I and Case II shown in both Fig. 4 and Fig. 5 are tiny for large $P_s$. Besides, the outage throughputs achieved by $x_1'$ and $x_{d_1}$ are much less than the other signals, and thus imperfect SIC has a limited impact on the outage throughput.

Fig. 9 plots the coverage of $U_3$ versus the transmit power of BS. Specifically, the coverage of $U_3$ is defined as the maximum coverage radius that $U_2$ can achieve when the outage-based quality-of-service constraint of $U_3$ is met. Here, we set $d_{s1} = 50$ m, $d_{s2} = 55$ m and $d_{21} = 10$ m. The outage probability threshold is assumed to be $10^{-2}$. Note that the distance $d_{23}$ should satisfy $0$ m $< d_{23} < 10$ m due to $d_{23} < d_{21}$. Fig. 9 shows that the proposed scheme can achieve larger coverage of $U_3$ than the conventional D-CDRT scheme in the low-medium transmit power region, which is consistent with the results discussed in Fig. 3. Moreover, both the proposed scheme and the conventional D-CDRT scheme can attain the same maximum of the coverage of $U_3$ in the high transmit power region.

## B. Average SE

Fig. 10 shows the relationship between the average SE and the transmit power of BS. To investigate the average SE difference between NOMA-based schemes (i.e., the proposed scheme, D-CDRT [34] and CDRT [38]) and OMA-based schemes, we design two benchmarks using time division multiple access (TDMA) (i.e., OMA-I and OMA-II) for fair comparisons. Specifically, OMA-I divides the whole transmission period into seven phases and adopts TDMA to transmit six signals of the proposed scheme. Similarly, OMA-II completes the transmission of four signals in the conventional scheme by using five phases. In Fig. 10, the theoretical analysis results of the average SE for the proposed scheme are perfectly matched with the corresponding simulation ones. The analysis of SE

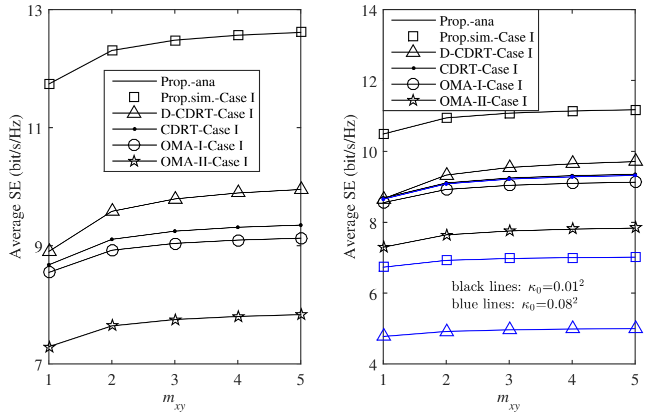


(a) Perfect SIC (b) Imperfect SIC

Fig. 11. Average SE versus the Nakagami-$m$ line-of-sight parameter (i.e., $m_{xy}$), with $P_s = 10$ dBm and the distance setting of Case I considered.

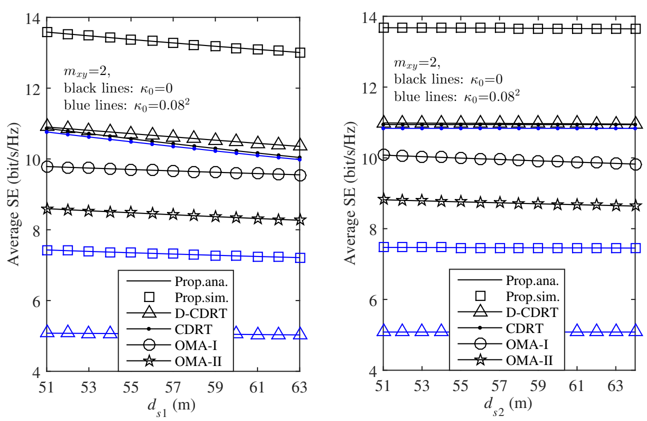


(a) (b)

Fig. 12. (a) Average SE according to $d_{s1}$, with $m_{xy} = 2$, $P_s = 10$ dBm, $d_{s2} = 65$ m, $d_{23} = 5$ m, and $d_{21} = 15$ m considered. (b) Average SE according to $d_{s2}$, with $m_{xy} = 2$, $P_s = 10$ dBm, $d_{s1} = 50$ m, $d_{23} = 5$ m, and $d_{21} = 15$ m considered.

scaling in Theorem 3 is also verified. The proposed scheme realizes the aggregation transmission of multiple data streams and outperforms the conventional scheme in terms of average SE under both perfect and imperfect SIC. When perfect SIC is performed, the proposed scheme and the D-CDRT scheme can achieve better average SE compared with CDRT and OMA-based schemes. Instead, the opposite results can be observed in the high transmit power region for imperfect SIC. This is because imperfect SIC significantly affects the average SE of the proposed scheme and the D-CDRT scheme, resulting in the existence of SE ceiling for large $P_s$. Moreover, since Case II has better channel qualities than Case I, the achievable average SE in Case II is superior to that in Case I.

Fig. 11 plots the average SE versus the Nakagami-$m$ line-of-sight parameter $m_{xy}$. From Fig. 11, we can observe that the proposed scheme can attain the best average SE performance compared with the other benchmarks under perfect SIC and imperfect SIC with a slight residual interference level. The average SE becomes better with the increase of $m_{xy}$ because larger $m_{xy}$ represents better channel quality. However, the increase rate of the average SE becomes smaller when $m_{xy}$ increases, especially under imperfect SIC. This is because the average SE is affected by the channel quality, power allocation coefficient and residual interference, and imperfect SIC becomes the main influencing factor when the channel quality is good enough and the power allocation coefficient setting is fixed.

Fig. 12 plots the average SE versus different $d_{s1}$ and $d_{s2}$. Without loss of generality, we set 51 m $< d_{s1} <$ 63 m and 51 m $< d_{s2} <$ 63 m in Fig. 12 (a) and Fig. 12 (b), respectively, which follows the construction rules of the triangle. In this figure, three observations can be drawn in the following. 1) The average SE achieved by all the schemes decreases as $d_{s1}$ becomes large. This is because the increase of $d_{s1}$ makes the channel quality of $h_{s1}$ worse, resulting in the achievable SE reduction of $x_1$ and $x_1'$ for all the schemes. Meanwhile, the change of $d_{s1}$ does not affect the achievable capacity of the other signals. 2) With the increase of $d_{s2}$, the average SE for NOMA-based schemes (i.e., the proposed scheme, D-CDRT and CDRT) remains almost constant under both perfect and imperfect SIC. This is because although large $d_{s2}$ can slightly reduce the achievable capacity of $x_2$ because of the worse $h_{s2}$, the average SE contributed by $x_2$ is very limited compared with all the other signals. 3) For OMA-based schemes, the SE realized by $x_2$ is crucial for the overall average SE. Therefore, the average SE for OMA-I and OMA-II decreases significantly as $d_{s2}$ increases due to the decrease of the achievable SE for $x_2$ caused by the increase of $d_{s2}$.

## VI. Conclusion

We studied a D2MD assisted cooperative NOMA system, where two CCUs and one CEU are paired as a D2MD cluster, and the BS can directly communicate with two CCUs and connect with the CEU with the help of one CCU. To further improve the reliability of the CEU and the SE, we design an adaptive aggregate transmission scheme by adopting dynamic superposition coding, pre-designing the decoding orders, and prior information cancellation. Moreover, we evaluated the performance for the proposed scheme in terms of outage probability, diversity order, outage throughput, ergodic sum capacity, average SE, and SE scaling over Nakagami-$m$ fading channels with both perfect and imperfect SIC. The correctness of the analytical results was validated through simulations. It is shown that the proposed scheme can achieve better outage performance of the CEU, outage throughput, and average SE under both perfect and imperfect SIC than the conventional D-CDRT scheme. When the level of residual interference is low, the proposed scheme can also attain superior SE than the OMA schemes. To further improve the achievable SE, we will investigate the related power allocation optimization problem and extend the proposed scheme to a multiple-input multiple-output scenario in future work.

## Appendix A
## Proof of Theorem 1

In the second phase, $U_1$ can adopt SIC to decode $x_1'$ after decoding $x_{d_1}$. Based on the proposed scheme, the outage probability for $U_1$ to decode $x_1'$ should be discussed in four cases (i.e., $A=0,1,2,3$) and given in (33).

If both $U_1$ and $U_2$ cannot decode $x_3$ successfully in the first phase (i.e., $A=0$), $U_2$ only transmits $x_{d_1}$ and $x_{d_3}$ via superposition coding in the second phase. Based on the proposed predetermined decoding order strategy, $U_2$ can use SIC to decode $x_1'$ after removing $x_{d_1}$. In this case, we can use $\gamma_{1,x_3}^{t_1}$, $\gamma_{2,x_3}^{t_1}$, $\gamma_{1,x_{d_1}}^{t_2,0}$ and $\gamma_{1,x_1'}^{t_2,0}$ to calculate the non-outage probability for $U_1$ to decode $x_1'$ as

$$\begin{aligned}&\mathbb{P}_{1,0}^{t_2,x_1'}\\&=\Pr\left(\gamma_{1,x_3}^{t_1}<\varphi_{x_3},\gamma_{2,x_3}^{t_1}<\varphi_{x_3},\gamma_{1,x_{d_1}}^{t_2,0}>\varphi_{x_{d_1}},\gamma_{1,x_1'}^{t_2,0}>\varphi_{x_1'}\right)\\&=\Pr\left(\xi_1^0<\lambda_{s1}<\phi_3,\lambda_{s1}\frac{\rho_s\phi_7^0}{\varphi_{x_1'}}-\phi_7^0>\lambda_{21}>\lambda_{s1}\rho_s\phi_5^0+\phi_5^0\right)\\&\quad\times F_{\lambda_{s2}}(\phi_3),\end{aligned}\tag{57}$$

where $\phi_3=\frac{\varphi_{x_3}}{\rho_s\left(a_3-(a_1+a_2)\varphi_{x_3}\right)}$, $\phi_5^A=\frac{\varphi_{x_{d_1}}}{\alpha\rho_s(b_1^A-(b_2^A+\varpi^A b_3^A)\varphi_{x_{d_1}})}$, $\phi_7^A=\frac{1}{(\kappa_{1,1}^{t_2,A}b_1^A+b_2^A+\varpi^A b_3^A)\alpha\rho_s}$ and $\xi_1^A=\min\left\{\frac{(\phi_5^A+\phi_7^A)\varphi_{x_1'}}{(\phi_7^A-\varphi_{x_1'}\phi_5^A)\rho_s},\phi_3\right\}$. The condition $\frac{\rho_s\phi_7^0}{\varphi_{x_1'}}-\phi_7^0>\lambda_{s1}\rho_s\phi_5^0+\phi_5^0$ should be satisfied, otherwise $\mathbb{P}_{1,0}^{t_2,x_1'}$ is always zero. Therefore, $\mathbb{P}_{1,0}^{t_2,x_1'}$ in (57) can be rewritten as

$$\begin{aligned}\mathbb{P}_{1,0}^{t_2,x_1'}=&\int_{\xi_1^0}^{\phi_3}\int_{\rho_s\phi_5^0x+\phi_5^0}^{\rho_s\phi_7^0x/\varphi_{x_1'}-\phi_7^0}f_{\lambda_{s1}}(x)f_{\lambda_{21}}(y)dxdy\\&\times F_{\lambda_{s2}}(\phi_3)\delta\left(\phi_7^0-\varphi_{x_1'}\phi_5^0\right),\end{aligned}\tag{58}$$

where the PDF of the channel gain $\lambda_{xy}$ is $f_{\lambda_{xy}}(z)=\left(\frac{zm_{xy}}{\Omega_{xy}}\right)^{m_{xy}}\frac{1}{\Gamma(m_{xy})}\exp\left(-\frac{zm_{xy}}{\Omega_{xy}}\right)$, and the step function $\delta(z)$ are zero and one for $z\le 0$ and $z>0$, respectively. Using (26) and some integral calculations, we can calculate $\mathbb{P}_{1,0}^{t_2,x_1'}$ as

$$\begin{aligned}\mathbb{P}_{1,0}^{t_2,x_1'}=&\Bigg\{\Delta_{j_1}^0\left(\mathcal{L}_1\left(\phi_3,j_1+m_{s1}-1,\frac{m_{21}\phi_5^0\rho_s}{\Omega_{21}}+\frac{m_{s1}}{\Omega_{s1}}\right)\right.\\&\left.-\mathcal{L}_1\left(\xi_1^0,j_1+m_{s1}-1,\frac{m_{21}\phi_5^0\rho_s}{\Omega_{21}}+\frac{m_{s1}}{\Omega_{s1}}\right)\right)\\&-\Delta_{j_2}^0\left(\mathcal{L}_1\left(\phi_3,j_2+m_{s1}-1,\frac{m_{21}\rho_s\phi_7^0}{\Omega_{21}\varphi_{x_1'}}+\frac{m_{s1}}{\Omega_{s1}}\right)\right.\\&\left.-\mathcal{L}_1\left(\xi_1^0,j_2+m_{s1}-1,\frac{m_{21}\rho_s\phi_7^0}{\Omega_{21}\varphi_{x_1'}}+\frac{m_{s1}}{\Omega_{s1}}\right)\right)\Bigg\}\\&\times F_{\lambda_{s2}}(\phi_3)\,\delta\left(\phi_7^0-\varphi_{x_1'}\phi_5^0\right),\end{aligned}\tag{59}$$

where $\Delta_{j_1}^A=\sum_{j=0}^{m_{21}-1}\sum_{j_1=0}^{j}\binom{j}{j_1}\left(\frac{m_{21}\phi_5^A}{\Omega_{21}}\right)^j\frac{{m_{s1}}^{m_{s1}}}{{\Omega_{s1}}^{m_{s1}}\Gamma(m_{s1})}/j!\times(\rho_s)^{j_1}\exp\left(-\frac{m_{21}\phi_5^A}{\Omega_{21}}\right)$ and $\Delta_{j_2}^A=\sum_{j=0}^{m_{21}-1}\sum_{j_2=0}^{j}\binom{j}{j_2}/j!\times\left(\frac{m_{21}\phi_7^A}{\Omega_{21}}\right)^j\left(\frac{\rho_s}{\varphi_{x_1'}}\right)^{j_2}(-1)^{j-j_2}\frac{{m_{s1}}^{m_{s1}}}{{\Omega_{s1}}^{m_{s1}}\Gamma(m_{s1})}\exp\left(\frac{m_{21}\phi_7^A}{\Omega_{21}}\right)$.

Similarly, if $A=1$, $U_2$ will broadcast the combination of $x_3$, $x_{d_1}$ and $x_{d_3}$ in the second phase. Therefore, $U_1$ decodes $x_{d_1}$ and $x_1'$ sequentially by treating $x_{d_3}$ and $x_3$ as noise. Based on this, using $\gamma_{1,x_3}^{t_1}$, $\gamma_{2,x_3}^{t_1}$, $\gamma_{1,x_{d_1}}^{t_2,1}$ and $\gamma_{1,x_1'}^{t_2,1}$, we can write $\mathbb{P}_{1,1}^{t_2,x_1'}$ for $A=1$ as

$$\begin{aligned}&\mathbb{P}_{1,1}^{t_2,x_1'}\\&=\Pr\left(\gamma_{1,x_3}^{t_1}<\varphi_{x_3},\gamma_{2,x_3}^{t_1}>\varphi_{x_3},\gamma_{1,x_{d_1}}^{t_2,1}>\varphi_{x_{d_1}},\gamma_{1,x_1'}^{t_2,1}>\varphi_{x_1'}\right)\\&=\Pr\left(\xi_1^1<\lambda_{s1}<\phi_3,\lambda_{s1}\frac{\rho_s\phi_7^1}{\varphi_{x_1'}}-\phi_7^1>\lambda_{21}>\lambda_{s1}\rho_s\phi_5^1+\phi_5^1\right)\\&\quad\times(1-F_{\lambda_{s2}}(\phi_3))\,\delta(\phi_7^1-\varphi_{x_1'}\phi_5^1)\\&=\mathbb{P}_{1,0}^{t_2,x_1'}\left(\xi_1^0\to\xi_1^1,\phi_7^0\to\phi_7^1,\phi_5^0\to\phi_5^1\right)\frac{(1-F_{\lambda_{s2}}(\phi_3))}{F_{\lambda_{s2}}(\phi_3)}.\end{aligned}\tag{60}$$

When $A=2$, $U_1$ can decode $x_3$ successfully while $U_2$ cannot decode $x_3$ in the first phase. Therefore, $U_2$ transmits the combination of $x_{d_1}$ and $x_{d_3}$ in the second phase. In this case, $U_1$ decodes $x_{d_1}$ and $x_1'$ sequentially by treating $x_{d_3}$ as noise. Based on this, we can use $\gamma_{1,x_3}^{t_1}$, $\gamma_{2,x_3}^{t_1}$, $\gamma_{1,x_{d_1}}^{t_2,2}$ and $\gamma_{1,x_1'}^{t_2,2}$ to calculate the non-outage probability for $U_1$ to decode $x_1'$ as

$$\begin{aligned}&\mathbb{P}_{1,2}^{t_2,x_1'}\\&=\Pr\left(\gamma_{1,x_3}^{t_1}>\varphi_{x_3},\gamma_{2,x_3}^{t_1}<\varphi_{x_3},\gamma_{1,x_{d_1}}^{t_2,2}>\varphi_{x_{d_1}},\gamma_{1,x_1'}^{t_2,2}>\varphi_{x_1'}\right)\\&=\Pr\left(\lambda_{s1}>\phi_3,\lambda_{s1}\frac{\rho_s\phi_7^2}{\varphi_{x_1'}}-\phi_7^2>\lambda_{21}>\lambda_{s1}\rho_s\phi_5^2+\phi_5^2\right)\\&\quad\times F_{\lambda_{s2}}(\phi_3)\delta\left(\phi_7^2-\varphi_{x_1'}\phi_5^2\right),\end{aligned}\tag{61}$$

Similar to (58), we can use (31) and some integral calculations to rewrite (61) as

$$\begin{aligned}\mathbb{P}_{1,2}^{t_2,x_1'}=&\Bigg\{\Delta_{j_1}^2\mathcal{L}_2\left(\xi_2^2,m_{s1}+j_1-1,\frac{m_{21}\rho_s\phi_5^2}{\Omega_{21}}+\frac{m_{s1}}{\Omega_{s1}}\right)\\&-\Delta_{j_2}^2\mathcal{L}_2\left(\xi_2^2,m_{s1}+j_2-1,\frac{m_{21}\rho_s}{\Omega_{21}}\frac{\phi_7^2}{\varphi_{x_1'}}+\frac{m_{s1}}{\Omega_{s1}}\right)\Bigg\}\\&\times F_{\lambda_{s2}}(\phi_3)\,\delta\left(\phi_7^2-\varphi_{x_1'}\phi_5^2\right),\end{aligned}\tag{62}$$

where $\xi_2^A=\max\left\{\frac{(\phi_5^A+\phi_7^A)\varphi_{x_1'}}{(\phi_7^A-\varphi_{x_1'}\phi_5^A)\rho_s},\phi_3\right\}$.

Similarly, $U_1$ can decode $x_{d_1}$ and $x_1'$ sequentially in the second phase by treating $x_{d_3}$ as noise when both $U_1$ and $U_2$ can decode $x_3$ successfully (i.e., $A=3$) in the first phase. This is because $U_1$ can use the known signal of $x_3$ to remove the corresponding interference caused by $x_3$. Following the same steps in (62), we can use $\gamma_{1,x_3}^{t_1}$, $\gamma_{2,x_3}^{t_1}$, $\gamma_{1,x_{d_1}}^{t_2,3}$ and $\gamma_{1,x_1'}^{t_2,3}$ to obtain $\mathbb{P}_{1,3}^{t_2,x_1'}$ as

$$\begin{aligned}&\mathbb{P}_{1,3}^{t_2,x_1'}\\&=\Pr\left(\gamma_{1,x_3}^{t_1}>\varphi_{x_3},\gamma_{2,x_3}^{t_1}>\varphi_{x_3},\gamma_{1,x_{d_1}}^{t_2,3}>\varphi_{x_{d_1}},\gamma_{1,x_1'}^{t_2,3}>\varphi_{x_1'}\right)\\&=\Pr\left(\xi_1^1<\lambda_{s1}>\phi_3,\lambda_{s1}\frac{\rho_s\phi_7^3}{\varphi_{x_1'}}-\phi_7^3>\lambda_{21}>\lambda_{s1}\rho_s\phi_5^3+\phi_5^3\right)\\&\quad\times(1-F_{\lambda_{s2}}(\phi_3))\,\delta(\phi_7^3-\varphi_{x_1'}\phi_5^3)\\&=\mathbb{P}_{1,2}^{t_2,x_1'}\left(\xi_2^2\to\xi_2^3,\phi_5^2\to\phi_5^3,\phi_7^2\to\phi_7^3\right)\frac{(1-F_{\lambda_{s2}}(\phi_3))}{F_{\lambda_{s2}}(\phi_3)}.\end{aligned}\tag{63}$$

Substituting (59), (60), (62) and (63) into (33), we obtain $P_{1,\mathrm{out}}^{t_2,x_1'}$.

The analytical results in Theorem 1 can be used to minimize the outage probability for $U_1$ to decode $x_1'$ by formulating the optimization problem and designing the power allocation coefficient.

## APPENDIX B
## PROOF OF THEOREM 2

When the variable $z$ satisfies $z \to 0$, we can obtain the approximation of $\exp(-z) \to 1-z$ by using the Maclaurin series [36]. Based on this, the CDF function in (20) with $z \to 0$ can be approximated as

$$F_{\lambda_{xy}}(z) = \frac{1}{m_{xy}!}\left(\frac{z m_{xy}}{\Omega_{xy}}\right)^{m_{xy}}. \tag{64}$$

Using (19), (21), (22), (25), (33), (36) and (64), we can respectively approximate $P_{1,\mathrm{out}}^{t_1,x_1}$, $P_{2,\mathrm{out}}^{t_1,x_2}$, $P_{3,\mathrm{out}}^{t_2,x_3}$, $P_{1,\mathrm{out}}^{t_2,x_{d_1}}$, $P_{1,\mathrm{out}}^{t_2,x_1'}$ and $P_{3,\mathrm{out}}^{t_2,x_{d_3}}$ for high SNR region (i.e., $\rho_s \to \infty$) as

$$P_{1,\mathrm{out}}^{t_1,x_1} \approx \frac{1}{m_{s1}}!\left(\frac{m_{s1}\tilde{\phi}_1}{\Omega_{s1}}\right)^{m_{s1}}, \tag{65}$$

$$P_{2,\mathrm{out}}^{t_1,x_2} \approx \frac{1}{m_{s2}!}\left(\frac{m_{s2}\tilde{\phi}_2}{\Omega_{s2}}\right)^{m_{s2}}, \tag{66}$$

$$P_{3,\mathrm{out}}^{t_2,x_3} \approx \frac{1}{m_{s2}!}\left(\frac{\phi_3 m_{s2}}{\Omega_{s2}}\right)^{m_{s2}} + \frac{1}{m_{23}!}\left(\frac{\tilde{\phi}_3^3 m_{23}}{\Omega_{23}}\right)^{m_{23}}, \tag{67}$$

$$\begin{aligned} P_{1,\mathrm{out}}^{t_2,x_{d_1}} \approx & 1 - \frac{{m_{s1}}^{m_{s1}}}{{\Omega_{s1}}^{m_{s1}}\Gamma(m_{s1})}\sum\nolimits_{i=0}^{m_{21}-1}\left(\frac{m_{21}\rho_s\phi_5^3}{\Omega_{21}}\right)^i \\ & \times\frac{(m_{s1}+i-1)!}{i!}\left(\frac{m_{s1}}{\Omega_{s1}}+\frac{m_{21}\rho_s\phi_5^3}{\Omega_{21}}\right)^{-m_{s1}-i}, \end{aligned} \tag{68}$$

$$\begin{aligned} P_{1,\mathrm{out}}^{t_2,x_1'} \approx & 1 - \frac{{m_{s1}}^{m_{s1}}}{{\Omega_{s1}}^{m_{s1}}\Gamma(m_{s1})}\sum\nolimits_{i=0}^{m_{21}-1}\frac{(m_{s1}+i-1)!}{i!} \\ & \times\left(\frac{m_{21}\rho_s}{\Omega_{21}}\right)^i\left\{\left(\phi_5^3\right)^i\left(\frac{m_{s1}}{\Omega_{s1}}+\frac{m_{21}\rho_s\phi_5^3}{\Omega_{21}}\right)^{-m_{s1}-i}\right. \\ & \left.-\left(\frac{\phi_7^3}{\varphi_{x_1'}}\right)^i\left(\frac{m_{s1}}{\Omega_{s1}}+\frac{m_{21}\rho_s\phi_7^3}{\Omega_{21}\varphi_{x_1'}}\right)^{-m_{s1}-i}\right\}, \end{aligned} \tag{69}$$

$$\begin{aligned} P_{3,\mathrm{out}}^{t_2,x_{d_3}} \approx & 1 + \zeta_1\zeta_3\left(\left(\tilde{\phi}_5^3\right)^{m_{23}} - \left(\tilde{\phi}_5^1\right)^{m_{23}}\right) \\ & + \zeta_2\zeta_3\left(\left(\tilde{\phi}_5^3\right)^{m_{23}} - \left(\tilde{\phi}_4^2\right)^{m_{23}}\right) - \zeta_3\left(\tilde{\phi}_5^3\right)^{m_{23}} \\ & + \zeta_1\zeta_2\zeta_3\left(\left(\tilde{\phi}_5^1\right)^{m_{23}} + (\tilde{\phi}_4^2)^{m_{23}} - (\tilde{\phi}_4^0)^{m_{23}}\right. \\ & \left. - \left(\tilde{\phi}_5^3\right)^{m_{23}}\right), \end{aligned} \tag{70}$$

where $\zeta_1 = \left(\frac{\phi_3 m_{s1}}{\Omega_{s1}}\right)^{m_{s1}}/m_{s1}!$, $\zeta_2 = \left(\frac{\phi_3 m_{s2}}{\Omega_{s2}}\right)^{m_{s2}}/m_{s2}!$ and $\zeta_3 = \left(\frac{m_{23}}{\Omega_{23}}\right)^{m_{23}}/m_{23}!$.

The diversity order corresponding to the outage probability $P_{\mathrm{out}}$ can be defined as

$$\mathcal{D}\left(P_{\mathrm{out}}\right) = -\lim_{\rho_s\to\infty}\frac{\log P_{\mathrm{out}}}{\log\rho_s}. \tag{71}$$

Therefore, substituting (65)-(70) into (71), we have $\mathcal{D}\left(P_{1,\mathrm{out}}^{t_1,x_1}\right) = \mathcal{D}\left(P_{2,\mathrm{out}}^{t_1,x_2}\right) = \mathcal{D}\left(P_{3,\mathrm{out}}^{t_2,x_3}\right) = \mathcal{D}\left(P_{3,\mathrm{out}}^{t_2,x_{d_3}}\right) = 1$ and $\mathcal{D}\left(P_{1,\mathrm{out}}^{t_2,x_1'}\right) = \mathcal{D}\left(P_{1,\mathrm{out}}^{t_2,x_{d_1}}\right) = 0$.

The analytical results verify that the data streams $x_1'$ and $x_{d_1}$ achieve the diversity order of zero due to the inter-channel interference. However, the data streams $x_1$, $x_2$, $x_3$, and $x_{d_3}$ will not suffer from the inter-channel interference, and thus they can achieve the diversity order of one. In practical applications, the power allocation coefficients related to data streams $x_1$, $x_2$, $x_3$, and $x_{d_3}$ should be reasonably designed to avoid the waste of power resources while ensuring the outage performance, because the outage probabilities corresponding to these data streams have error floors when the transmit SNR becomes large.

## APPENDIX C
## PROOF OF THEOREM 3

The following approximations, i.e., $\exp(-z) \approx 1-z$ and $\mathrm{Ei}(x) \approx E^* + z + \ln(-z)$ always hold for $z \to 0$, where $E^*$ denotes the Euler constant [36]. When the proposed scheme performs perfect SIC, applying the above approximations to (46) and (55), we can obtain $\bar{C}_{x_1} \sim \frac{1}{2}\log_2\rho_s$ and $\bar{C}_{x_{d_3}}^3 \sim \frac{1}{2}\log_2\rho_s$ in the high transmit SNR region. Due to the SC characteristics of NOMA, the ergodic capacities for the other signals are interference limited, and they gradually become constant with the increase of $\rho_s$. Specifically, if $\rho_s \to \infty$, we can use (14), (16), (17) and (18) to obtain the following approximations

$$C_{x_1'}^3 \approx \mathbb{E}\left\{\frac{1}{2}\log_2\left(1+\frac{\lambda_{s1}}{\lambda_{21}b_2^A\alpha}\right)\right\}, \tag{72a}$$

$$\bar{C}_{x_2} \approx \frac{1}{2}\log_2\left(1+\frac{a_2}{a_1}\right), \tag{72b}$$

$$C_{x_{d_1}}^3 \approx \mathbb{E}\left\{\frac{1}{2}\log_2\left(1+\min\left\{\frac{\lambda_{21}b_1^3\alpha}{\lambda_{s1}+\lambda_{21}b_2^3\alpha}, \frac{b_1^3}{b_2^3+b_3^3}\right\}\right)\right\}, \tag{72c}$$

$$\bar{C}_{x_3}^3 \approx \frac{1}{2}\log_2\left(1+\min\left\{\frac{a_3}{a_1+a_2}, \frac{b_3^3}{b_2^3}\right\}\right). \tag{72d}$$

Based on the above analysis and (42), the SE scaling of the proposed scheme with perfect SIC is $\log_2\rho_s$.

Moreover, imperfect SIC causes the residual interference, and thus the ergodic capacity approximations of the proposed scheme for $\rho_s \to \infty$ can be written as

$$\bar{C}_{x_1} \approx \frac{1}{2}\log_2\left(1+\frac{a_1}{\kappa_{1,2}^{t_1}a_2+\kappa_{1,3}^{t_1}a_3}\right), \tag{73a}$$

$$\bar{C}_{x_2} \approx \frac{1}{2}\log_2\left(1+\frac{a_2}{a_1+\kappa_{1,1}^{t_1}a_3}\right), \tag{73b}$$

$$\bar{C}_{x_3}^3 \approx \frac{1}{2}\log_2\left(1+\min\left\{\frac{a_3}{(a_1+a_2)}, \frac{b_3^3}{(\kappa_{3,1}^{t_2,3}b_1^3+b_2^3)}\right\}\right), \tag{73c}$$

$$C_{x_1'}^3 \approx \mathbb{E}\left\{\frac{1}{2}\log_2\left(1+\frac{\lambda_{s1}}{\lambda_{21}\left(\kappa_{1,1}^{t_2,A}b_1^A+b_2^A+\varpi^A b_3^A\right)\alpha}\right)\right\}, \tag{73d}$$

$$C_{x_{d_1}}^3 \approx \mathbb{E}\left\{\frac{1}{2}\log_2\left(1+\min\left\{\frac{\lambda_{21}b_1^3\alpha}{\lambda_{s1}+\lambda_{21}b_2^3\alpha}, \frac{b_1^3}{b_2^3+b_3^3}\right\}\right)\right\}, \tag{73e}$$

$$C_{x_{d_3}}^3 \approx \frac{1}{2}\log_2\left(1+\frac{b_2^3}{(\kappa_{3,2}^{t_2,3}b_1^3+\kappa_{3,3}^{t_2,3}b_3^3)}\right). \tag{73f}$$

Combining (42) and (73), we obtain that the SE scaling becomes zero when the proposed scheme performs imperfect SIC.

Based on the above discussions, the corresponding rationale can be summarized as follows. When perfect SIC is performed, only $x_1$ and $x_{d_3}$ are not affected by the inter-user interference or the inter-channel interference. Therefore, the growth rate of $\bar{C}_{x_1}$ and $\bar{C}^3_{x_{d_3}}$ with the increase of $\rho_s$ is $\frac{1}{2}\log_2\rho_s$ in the high SNR region, while the ergodic capacities for the other signals are almost constant. Conversely, if imperfect SIC is performed, the transmissions of all the signals are affected by interference such as inter-user interference, inter-channel interference, and residual interference. Therefore, the SE scaling becomes zero. The analytical results in Theorem 3 can provide theoretical support for effectively improving the SE under high SNR condition.

## REFERENCES

[1] W. Ahsan, W. Yi, Z. Qin, Y. Liu and A. Nallanathan, "Resource allocation in uplink NOMA-IoT networks: A reinforcement-learning approach," *IEEE Trans. Commun.*, early access, Mar. 18, 2021, doi: 10.1109/TWC.2021.3065523.

[2] S. K. Sharma and X. Wang, "Toward massive machine type communications in ultra-dense cellular IoT networks: Current issues and machine learning-assisted solutions, " *IEEE Commun. Surveys Tuts.*, vol. 22, no. 1, pp. 426–471, 1st Quart., 2020.

[3] Z. Ding, X. Lei, G. K. Karagiannidis, R. Schober, J. Yuan, and V. Bhargava, "A survey on non-orthogonal multiple access for 5G networks: Research challenges and future trends," *IEEE J. Sel. Areas Commun.*, vol. 35, no. 10, pp. 2181–2195, Oct. 2017.

[4] L. Dai, B. Wang, Z. Ding, Z. Wang, S. Chen, and L. Hanzo, "A survey of non-orthogonal multiple access for 5G," *IEEE Commun. Surveys Tuts.*, vol. 20, no. 3, pp. 2294–2323, 3rd Quart., 2018.

[5] Y. Liu, Z. Qin, M. Elkashlan, Z. Ding, A. Nallanathan, and L. Hanzo, "Nonorthogonal multiple access for 5G and beyond," *Proc. IEEE*, vol. 105, no. 12, pp. 2347–2381, Dec. 2017.

[6] N. Zhao, W. Wang, J. Wang, Y. Chen, Y. Lin, Z. Ding, and N. C. Beaulieu, "Joint beamforming and jamming optimization for secure transmission in MISO-NOMA networks," *IEEE Trans. Commun.*, vol. 67, no. 3, pp. 2294–2305, Mar. 2019.

[7] Z. Ding, F. Adachi, and H. V. Poor, "The application of MIMO to non-orthogonal multiple access," *IEEE Trans. Wireless Commun.*, vol. 15, no. 1, pp. 537–552, Jan. 2016.

[8] Y. Xu, J. Cheng, G. Wang and V. C. M. Leung, "Adaptive coordinated direct and relay transmission for NOMA networks: A joint downlink-uplink scheme," *IEEE Trans. Wireless Commun.*, vol. 20, no. 7, pp. 4328-4346, Jul. 2021.

[9] J. Zhao, Y. Liu, K. K. Chai, Y. Chen, and M. Elkashlan, "Joint subchannel and power allocation for NOMA enhanced D2D communications, " *IEEE Trans. Commun.*, vol. 65, no. 11, pp. 5081–5094, Nov. 2017.

[10] L. Pei, Z. Yang, C. Pan, W. Huang, M. Chen, M. Elkashlan, and A. Nallanathan, "Energy-efficient D2D communications underlaying NOMA-based networks with energy harvesting," *IEEE Commun. Lett.*, vol. 22, no. 5, pp. 914–917, May 2018.

[11] Y. Pan, C. Pan, Z. Yang, and M. Chen, "Resource allocation for D2D communications underlaying a NOMA-based cellular network," *IEEE Wireless Commun. Lett.*, vol. 7, no. 1, pp. 130–133, Feb. 2018.

[12] H. Zheng, S. Hou, H. Li, Z. Song, and Y. Hao, "Power allocation and user clustering for uplink MC-NOMA in D2D underlaid cellular networks, " *IEEE Wireless Commun. Lett.*, vol. 7, no. 6, pp. 1030–1033, Dec. 2018.

[13] Y. Dai, M. Sheng, J. Liu, N. Cheng, X. Shen, and Q. Yang, "Joint mode selection and resource allocation for D2D-enabled NOMA cellular networks," *IEEE Trans. Veh. Technol.*, vol. 68, no. 7, pp. 6721–6733, Jul. 2019.

[14] R. Li, P. Hong, K. Xue, M. Zhang and T. Yang, "Resource allocation for uplink NOMA-based D2D communication in energy harvesting scenario: A two-stage game approach," *IEEE Trans. Wireless Commun.*, early access, Aug. 2021, doi: 10.1109/TWC.2021.3100567.

[15] M. Sun, X. Xu, X. Tao, P. Zhang and V. C. M. Leung, "NOMA-based D2D-enabled traffic offloading for 5G and beyond networks employing licensed and unlicensed access," *IEEE Trans. Wireless Commun.*, vol. 19, no. 6, pp. 4109-4124, Jun. 2020.

[16] Z. Ding, M. Peng, and H. V. Poor, "Cooperative non-orthogonal multiple access in 5G systems," *IEEE Commun. Lett.*, vol. 19, no. 8, pp. 1462–1465, Aug. 2015.

[17] Z. Ding, H. Dai, and H. V. Poor, "Relay selection for cooperative NOMA," *IEEE Wireless Commun. Lett.*, vol. 5, no. 4, pp. 416–419, Aug. 2016.

[18] Y. Liu, Z. Ding, M. Elkashlan, and H. V. Poor, "Cooperative nonorthogonal multiple access with simultaneous wireless information and power transfer," *IEEE J. Sel. Areas Commun.*, vol. 34, no. 4, pp. 938–953, Apr. 2016.

[19] L. Lv, J. Chen, Q. Ni, and Z. Ding, "Design of cooperative non-orthogonal multicast cognitive multiple access for 5G systems: User scheduling and performance analysis," *IEEE Trans. Commun.*, vol. 65, no. 6, pp. 2641–2656, Jun. 2017.

[20] Y. Cao, N. Zhao, G. Pan, Y. Chen, L. Fan, M. Jin, and M.-S. Alouini, "Secrecy analysis for cooperative NOMA networks with multi-antenna full-duplex relay," *IEEE Trans. Commun.*, vol. 67, no. 8, pp. 5574–5587,Aug. 2019.

[21] C. Zhong and Z. Zhang, "Non-orthogonal multiple access with cooperative full-duplex relaying, " *IEEE Commun. Lett.*, vol. 20, no. 12, pp. 2478–2481, Dec. 2016.

[22] Q. Si, M. Jin, T. A. Tsiftsis, N. Zhao and X. Wang, "Cooperative SM-based NOMA scheme with SWIPT," *IEEE Trans. Veh. Technol.*, vol. 70, no. 6, pp. 6195-6199, Jun. 2021.

[23] Y. Xu, C. Shen, Z. Ding, X. Sun, S. Yan, G. Zhu, and Z. Zhong, "Joint beamforming and power-splitting control in downlink cooperative SWIPT NOMA systems," *IEEE Trans. Signal Process.*, vol. 65, no. 18, pp. 4874–4886, Sep. 2017.

[24] L. Qian, Y. Wu, J. Ouyang, Z. Shi, B. Lin, and W. Jia, "Latency optimization for cellular assisted mobile edge computing via non-orthogonal multiple access," *IEEE Trans. Veh. Technol.*, vol. 69, no. 5, pp. 5494–5507, May 2020.

[25] J. Bae and Y. Han, "Joint power and time allocation for two-way cooperative NOMA," *IEEE Trans. Veh. Technol.*, vol. 68, no. 12, pp. 12443–12447, Dec. 2019.

[26] Y. Yuan, Y. Xu, Z. Yang, P. Xu, and Z. Ding, "Energy efficiency optimization in full-duplex user-aided cooperative SWIPT NOMA systems," *IEEE Trans. Commun.*, vol. 67, no. 8, pp. 5753–5767, Aug. 2019.

[27] F. Zhou, Z. Chu, H. Sun, R. Q. Hu, and L. Hanzo, "Artificial noise aided secure cognitive beamforming for cooperative MISO-NOMA using SWIPT," *IEEE J. Sel. Areas Commun.*, vol. 36, no. 4, pp. 918–931, Apr. 2018.

[28] Y. Wu, L. Qian, H. Mao, X. Yang, H. Zhou, and X. Shen,"Optimal power allocation and scheduling for non-orthogonal multiple access relay-assisted networks" *IEEE Trans. Mobile Comput.*, vol. 17, no. 11, pp. 2591–2606, Nov. 2018.

[29] Z. Zhang, Z. Ma, M. Xiao, Z. Ding, and P. Fan, "Full-duplex device-to device-aided cooperative nonorthogonal multiple access, " *IEEE Trans. Veh. Technol.*, vol. 66, no. 5, pp. 4467–4471, May 2017.

[30] J.-B. Kim, I.-H. Lee, and J. Lee, "Capacity scaling for D2D aided cooperative relaying systems using NOMA," *IEEE Wireless Commun. Lett.*, vol. 7, no. 1, pp. 42–45, Feb. 2018.

[31] Y. Xu, G. Wang, B. Li, and S. Jia, "Performance of D2D aided uplink coordinated direct and relay transmission using NOMA," *IEEE Access*, vol. 7, pp. 151090–151102, Oct. 2019.

[32] R. Li, P. Hong, K. Xue and T. Yang, "A cooperative D2D content sharing scheme using NOMA under social ties," *IEEE Commun. Lett.*, early access, Jul. 2021, doi: 10.1109/LCOMM.2021.3097762.

[33] M. F. Kader, S. M. R. Islam and O. A. Dobre, "Simultaneous cellular and D2D communications exploiting cooperative uplink NOMA," *IEEE Commun. Lett.*, vol. 25, no. 6, pp. 1848-1852, Jun. 2021.

[34] L. Zou, J. Chen, L. Lv, and B. He, "Capacity enhancement of D2D aided coordinated direct and relay transmission using NOMA," *IEEE Commun. Lett.*, vol. 24, no. 10, pp. 2128–2132, Oct. 2020.

[35] P. Mach, Z. Becvar, and T. Vanek, "In-band device-to-device communication in OFDMA cellular networks: A survey and challenges," *IEEE Commun. Surveys Tuts.*, vol. 17, no. 4, pp. 1885–1922, 4th Quart., 2015.

[36] Y. Xu, J. Cheng, G. Wang and V. C. M. Leung, "Coordinated direct and relay transmission for multiuser networks: NOMA or hybrid multiple access?," *IEEE Wireless Commun. Lett.*, vol. 10, no. 5, pp. 976-980, May 2021.

[37] L. Lv, H. Jiang, Z. Ding, L. Yang, and J. Chen, "Secrecy-enhancing design for cooperative downlink and uplink NOMA with an untrusted relay," *IEEE Trans. Commun.*, vol. 68, no. 3, pp. 1698-1715, Mar. 2020.

[38] J. Kim and I. Lee, "Non-orthogonal multiple access in coordinated direct and relay transmission," *IEEE Commun. Lett.*, vol. 19, no. 11, pp. 2037–2040, Nov. 2015.

[39] I. S. Gradshteyn and I. M. Ryzhik, *Tables of Integrals, Series, and Products*, 7th ed. New York, NY, USA: Academic, 2007.

[40] Benedetto and E. Biglieri, *Principles of Digital Transmission: With Wireless Applications.* New York, NY, USA: Kluwer, 1999.

[41] X. Chen, R. Jia, and D. W. K. Ng, "On the design of massive non-orthogonal multiple access with imperfect successive interference cancellation," *IEEE Trans. Commun.*, vol. 67, no. 3, pp. 2539–2551, Mar. 2019.

**Yao Xu** received the B.S. degree in communication engineering from the Harbin Institute of Technology, China, in 2016, where he is currently pursuing the Ph.D. degree in information and communication engineering. From 2019 to 2020, he was a Visiting Student with the Department of Electrical and Computer Engineering, the University of British Columbia, Vancouver, BC, Canada. His research interests include non-orthogonal multiple access, cooperative energy-harvesting networks, and cooperative full-duplex networks.

**Jie Tang** (Senior Member, IEEE) received the B.Eng. degree in information engineering from the South China University of Technology, Guangzhou, China, in 2008, the M.Sc. degree (Hons.) in communication systems and signal processing from the University of Bristol, U.K., in 2009, and the Ph.D. degree from Loughborough University, Leicestershire, U.K., in 2012.

From 2003 to 2015, he was a Research Associate with the School of Electrical and Electronic Engineering, The University of Manchester, U.K. He is currently a Full Professor with the School of Electronic and Information Engineering, South China University of Technology, China. His current research centers around 5G and beyond mobile communications, including topics, such as massive MIMO, full-duplex communications, edge caching and fog networking, physical layer security, wireless power transfer, and mobile computing. He is a Senior Member of CIE and CIC. He was a co-recipient of the 2018 IEEE ICNC, 2018 CSPS, and 2019 IEEE WCSP Best Paper Award. He also served as the Track Co-Chair for IEEE VTC-Spring 2018, EAI GreeNets 2019, ICCC Workshop 2019, and ICCC 2020. He is serving as an Editor for IEEE WIRELESS COMMUNICATIONS LETTERS, IEEE ACCESS, and *EURASIP Journal on Wireless Communications and Networking*.

**Bo Li** (Member, IEEE) received the B.S. degree in communication engineering and the M.S. and Ph.D. degrees in information and communication engineering from the Harbin Institute of Technology, China, in 2007, 2009, and 2013, respectively. He was a Visiting Ph.D. Student with the School of EEE, Nanyang Technological University, Singapore, from 2012 to 2013. Since 2013, he has been an Associate Professor with the School of Information Science and Engineering, Harbin Institute of Technology. His research interests include physical layer network coding, mobile ad hoc networks, and adaptive modulation and coding.

**Nan Zhao** (Senior Member, IEEE) received the B.S. degree in electronics and information engineering, the M.E. degree in signal and information processing, and the Ph.D. degree in information and communication engineering from the Harbin Institute of Technology, Harbin, China, in 2005, 2007, and 2011, respectively. He is currently a Professor with the School of Information and Communication Engineering, Dalian University of Technology, Dalian, China, where he did a post-doctoral research from 2011 to 2013. He has published more than 90 articles in refereed journals and more than 90 papers in refereed international conferences. His recent research interests include interference alignment, cognitive radio, wireless power transfer, optical communications, and indoor localization. He is a Senior Member of the Chinese Institute of Electronics. In addition, he served as a Technical Program Committee (TPC) Member for many interferences, including Globecom, VTC, and WCSP. He serves as an Editor for IEEE WIRELESS COMMUNICATIONS LETTERS, IEEE ACCESS, *Wireless Networks*, the *Physical Communication*, the *AEU-International Journal of Electronics and Communications*, the *Ad Hoc & Sensor Wireless Networks*, and the *KSII Transactions on Internet and Information Systems*.

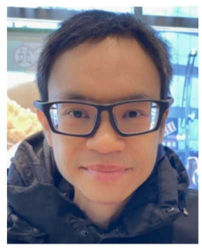

**Dusit Niyato** (Fellow, IEEE) received the B.E. degree from King Mongkut's Institute of Technology Ladkrabang (KMITL), Thailand, in 1999, and the Ph.D. degree in electrical and computer engineering from the University of Manitoba, Canada, in 2008. He is currently a Professor with the School of Computer Science and Engineering, Nanyang Technological University, Singapore. His research interests are in the areas of the Internet of Things (IoT), machine learning, and incentive mechanism design.

**Kai-Kit Wong** (Fellow, IEEE) received the B.Eng., M.Phil., and Ph.D. degrees in electrical and electronic engineering from The Hong Kong University of Science and Technology, Hong Kong, in 1996, 1998, and 2001, respectively. After graduation, he took up academic and research positions at The University of Hong Kong; Lucent Technologies; Bell-Labs, Holmdel; the Smart Antennas Research Group, Stanford University; and the University of Hull, U.K. He is currently the Chair of wireless communications with the Department of Electronic and Electrical Engineering, University College London, U.K. His current research interests include around 5G and beyond mobile communications, including topics such as massive MIMO, full-duplex communications, millimetre-wave communications, edge caching and fog networking, physical layer security, wireless power transfer and mobile computing, V2X communications, and of course cognitive radios. His few other unconventional research topics that he has set his heart on, including for example, fluid antenna communications systems, and team optimization. Dr. Wong is a fellow of IET. He was a co-recipient of the 2013 IEEE Signal Processing Letters Best Paper Award and the 2000 IEEE VTS Japan Chapter Award at the IEEE Vehicular Technology Conference in Japan, in 2000, and a few other international best paper awards. He is also on the editorial board of several international journals. He has been serving as a Senior Editor for IEEE COMMUNICATIONS LETTERS since 2012 and IEEE WIRELESS COMMUNICATIONS LETTERS since 2016. He is also an Area Editor of IEEE TRANSACTIONS ON WIRELESS COMMUNICATIONS. He had also previously served as an Associate Editor for IEEE SIGNAL PROCESSING LETTERS from 2009 to 2012 and an Editor for IEEE TRANSACTIONS ON WIRELESS COMMUNICATIONS from 2005 to 2011. He was also a Guest Editor of IEEE JOURNAL ON SELECTED AREAS IN COMMUNICATIONS Special Issue on Virtual MIMO in 2013. He is currently a Guest Editor of IEEE JOURNAL ON SELECTED AREAS IN COMMUNICATIONS Special Issue on Physical Layer Security for 5G.